Experimental investigation of the Ca-Mg-Zn system via diffusion couples and key experiments

Yinan Zhang

A Thesis
in

The Department
of
Mechanical and Industrial Engineering

Presented in Partial Fulfillment of the Requirements
for the Degree of Master of Applied Science (Mechanical Engineering) at
Concordia University
Montreal, Quebec, Canada

November 2010

CONCORDIA UNIVERSITY

School of Graduate Studies

By: Yinan Zhang

Entitled: Experimental Investigation of the Ca-Mg-Zn System via Diffusion Couples and Key Experiments

and submitted in partial fulfillment of the requirements for the degree of

Master of Applied Science

complies with the regulations of the University and meets the accepted standards with respect to originality and quality.

Signed by the final Examining Committee:

Dr. R.Sedaghati Chair

Dr. M.Pugh Examiner

Dr. A.Zsaki Examiner

Dr. M. Medraj Supervisor

Dr. P. Chartrand Supervisor

Approved by Dr. X.F. Xie
Chair of Department or Graduate Program Director

30th of Dec, 2010 Robin Drew
Dean of Faculty

ABSTRACT

Experimental investigation of the Ca-Mg-Zn system via diffusion couples and key experiments

Yinan Zhang

Nine diffusion couples and 32 key samples have been used to study the phase diagram of the Ca-Mg-Zn system at 335ºC and crystal structures of ternary intermetallics. Four ternary compounds have been found in this system: $Ca_3Mg_xZn_{15-x}$ ($4.6 \leqslant x \leqslant 12$ at 335ºC) (IM1); $Ca_{14.5}Mg_{15.8}Zn_{69.7}$ (IM2); $Ca_xMg_yZn_z$ (x = 8.2-9.1; y = 27.1-31.0; z = 60.8-64.7 at 335ºC) (IM3) and $Ca_{1.5}Mg_{55.3}Zn_{43.2}$ (IM4). Phase relations and solubility limits have been determined for binary and ternary compounds using Scanning Electron Microscopy, Electron Probe Microanalysis and X-ray Diffraction techniques. Crystal structures of the IM1 and IM3 ternary compounds have been studied by means of XRD, Transmission Electron Microscopy and Electron Back Scattered Diffraction. The refinement of the XRD patterns for IM1 ternary compound has been carried out by Rietveld analysis. XRD data has shown that this solid solution crystallizes in hexagonal structure having *P63/mmc* (194) space group and $Sc_3Ni_{11}Si_4$ prototype. The lattice parameters decrease linearly with decreasing Mg content obeying Vegard's law. The fractional atomic occupancy of 6h, 4f, 2b and 12k sites of this compound are function of Mg concentration. Focused Ion Beam has been used to lift Transmission Electron Microscopy specimen of the ternary compound and the hexagonal structure has been confirmed by means of Selected Area Electron Diffraction data. Based on the atomic occupancy results and the

crystallographic details, a three sublattice $(Ca)(Zn)(Mg,Zn)_4$ model is proposed for this compound.

Three binary compounds are found to have extended solid solubility into the ternary system. $CaZn_{11}$, $CaZn_{13}$ and Mg_2Ca are forming substitutional solid solutions where Mg substitutes Zn atoms in the first two compounds, and Zn substitutes both Ca and Mg atoms in Mg_2Ca. Based on the current experimental results, the isothermal section of Ca-Mg-Zn phase diagram at 335ºC has been constructed. The morphologies of diffusion couples have been studied in the Ca-Mg-Zn system at 335ºC. Depending on the terminal compositions of the diffusion couples, the morphology of the two-phase regions in the diffusion zone has: 'tooth-like' morphology or matrix phase with isolated and/or dendritic shape precipitates morphology.

ACKNOWLEDGEMENTS

First of all, I would like to express my deep gratitude and sincere appreciation to my supervisor, Professor Mamoun Medraj, for his advice, encouragement, critical suggestions and continuous support during my master study at Concordia University. It is my privilege and pleasure to work for him.

I would like to thank Research Associate, Dr. Dmytro Kenorkov, for his comments and constructive suggestions both in experimental works and technical writing.

I would also like to take the opportunity to thank Dr. Jian Li and Dr. Elhachmi Essadiqi from CANMET-MTL for their help with Focus Ion Beam-Transmission Electron Microscopy work. The help of Ms. Ming Wei and Mr. Alain Tessier from chemistry department of Concordia University in conducting the Inductively Coupled Plasma-Mass Spectrometry measurements is greatly appreciated. I would like to thank Mr. Lang Shi from Mcgill for his help with EPMA experiments. Also, a great thank is given to Dr. Florent Bridier, for his help and cooperation, the SEM/EDS and EBSD has been well carried out. Furthermore, I would like to thank Mr. Pierre Hovington from Hydro-Quebec research center for his help in sample preparation for Electron Back Scattered Diffraction analysis. I want to also thank my friend Guy-Joel Rocher for his constant help and suggestions.

I would like to thank the members of Dr. Medraj's research group for their kind help and support during my research. In addition, financial support from General Motors Canada Ltd. and NSERC through the CRD grant program is gratefully acknowledged.

I thank all the staff members of our department for their kind help in solving my academic and technical problems.

Special thanks is given to my family for their love, continuous support, understanding and constant encouragement.

TABLE OF CONTENTS

LIST OF ABBREVIATIONS

OM	Optical Microscopy
SEM	Scanning Electron Microscopy
EDS	Energy Dispersive X-ray Spectrometer
EPMA	Electron Probe Microanalysis
WDS	Wavelength Dispersive X-ray Spectrometry
XRD	X-ray Diffraction
EBSD	Electron Backscattered Diffraction
FIB	Focus Ion Beam
TEM	Transmission Electron Microscopy

CHAPTER 1

Introduction

As weight reduction is one of the major means available to improve fuel efficiency, magnesium-based alloys have attracted much attention as the lightest structural alloys for the aerospace and automotive applications. Mg-Al based alloys are one of the most important Mg alloys where the AM and AZ series can perform very well at room temperature. However, the precipitation of γ-$Al_{12}Mg_{17}$ phase is responsible for poor creep property of Al containing Mg-based alloys. Hence, a large amount of effort has been made to increase the service temperature of these alloys. The addition of Ca to the Al-Mg-Zn based alloys can be beneficial not only to keep the cost low but also to increase of grain boundary phases and improve the mechanical properties especially the creep resistance at elevated temperatures [1].

Furthermore, the addition of Ca element has been reported in recent years to be suitable to replace the cost intensive rare earth metals [2]. It is also well known that the addition of Ca up to 0.3 wt.% increases ductility through the grain size refinement [3]. Ca content in Mg alloys improves strength, castability, and creep and corrosion resistance [4]. In addition, it has been reported that another major alloying element Zn has significant amount of solid solubility in Mg. This results in improving solid solution strengthening in

Mg alloys. Zn also results in good balance of yield strength, increases fracture toughness of wrought magnesium alloys and reinforces the age hardening response [5]. Although many researchers have concentrated on the Mg-rich region, recently a biocompatible metallic glass has been found by Zberg et al. [6, 7] in Ca-Mg-Zn alloys containing approximately 28 at.% of Zn. This metallic glass shows a great potential for the development of biodegradable implants.

Phase diagram plays a significant role in basic materials research in fields such as solidification, crystal growth, joining, solid-state reaction, and phase transformation. It also serves as a blueprint for material design and processing variables to achieve the desired microstructures and mechanical properties [8, 9]. The properties of a material depend first on the phases and microstructural constituents that are present. The alloy systems containing several elements have complex phase relations. A Phase diagram is essential for better understanding and investigating these complex phase relationships.

The CALPHAD (Calculation of Phase Diagrams) method is based on the fact that a phase diagram is a representation of the thermodynamic properties of a system [10]. Thus, if the thermodynamic properties are known, it would be possible to calculate the multi-component phase diagram [11]. The Gibbs energy of a phase is described by a representative model that contains some experimental information such as melting, transformation temperatures, solubility, as well as thermodynamic properties. Experimental investigation of a multi-component phase diagram such as the Ca-Mg-Zn ternary system can be time-consuming and expensive. Therefore, CALPHAD method

offers a reliable and versatile alternative to generate phase diagrams, and requires key experiments that are identified using preliminary calculations to validate the thermodynamic models and to check inconsistencies in the reported experimental data. This combined approach of thermodynamic modeling and the experimental investigation is used in this research to provide consistent description of the phase equilibria in the Ca-Mg-Zn system at 335ºC.

Thermodynamic modeling of the Ca-Mg-Zn system was performed by Wasiur-Rahman and Medraj [12] through combining the thermodynamic descriptions of the constituent binaries and two ternary intermetallics using FactSage program [13]. They reported the calculated liquidus surface of the Ca-Mg-Zn system presented in Fig 1.1 with the experimental results obtained by Paris [14], and the calculated isothermal section of the Ca-Mg-Zn system at 335ºC as illustrated in Fig 1.2

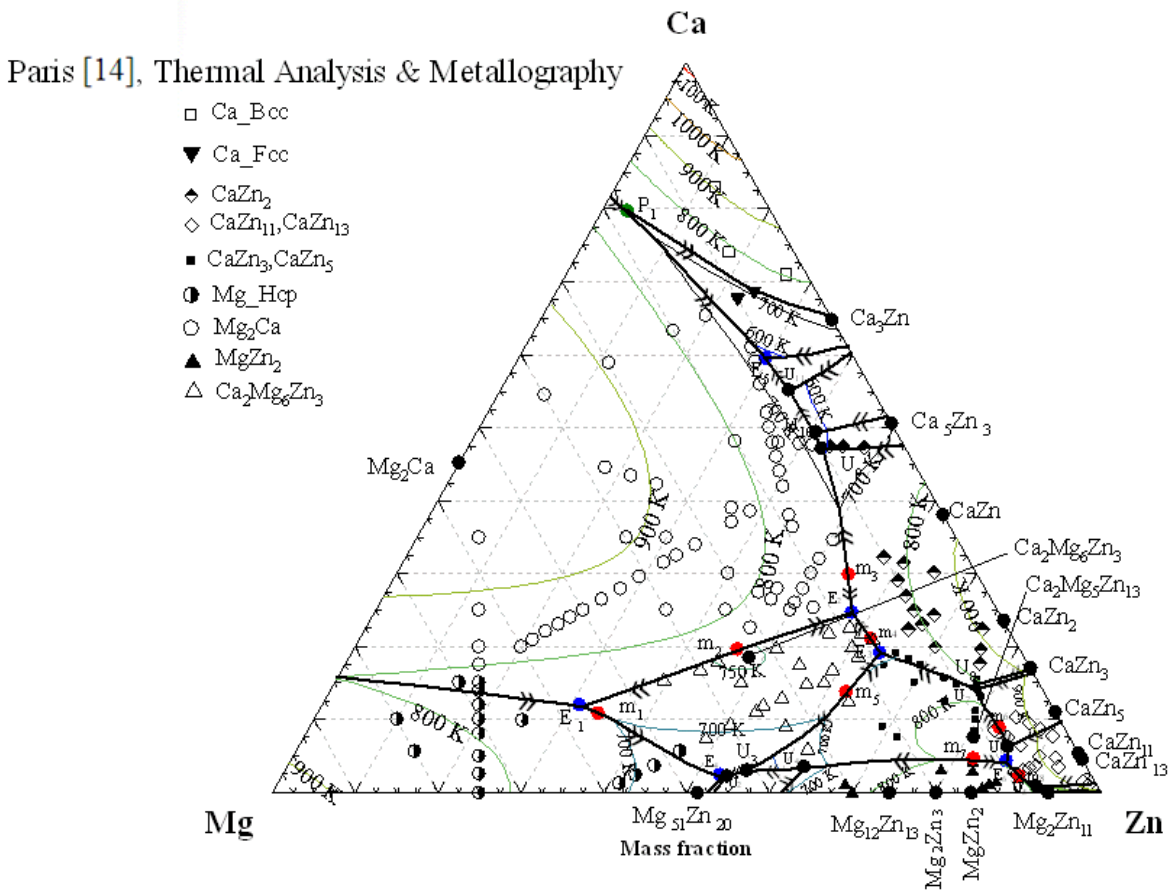

Fig 1.1: Calculated liquidus surface of the Ca-Mg-Zn system [12].

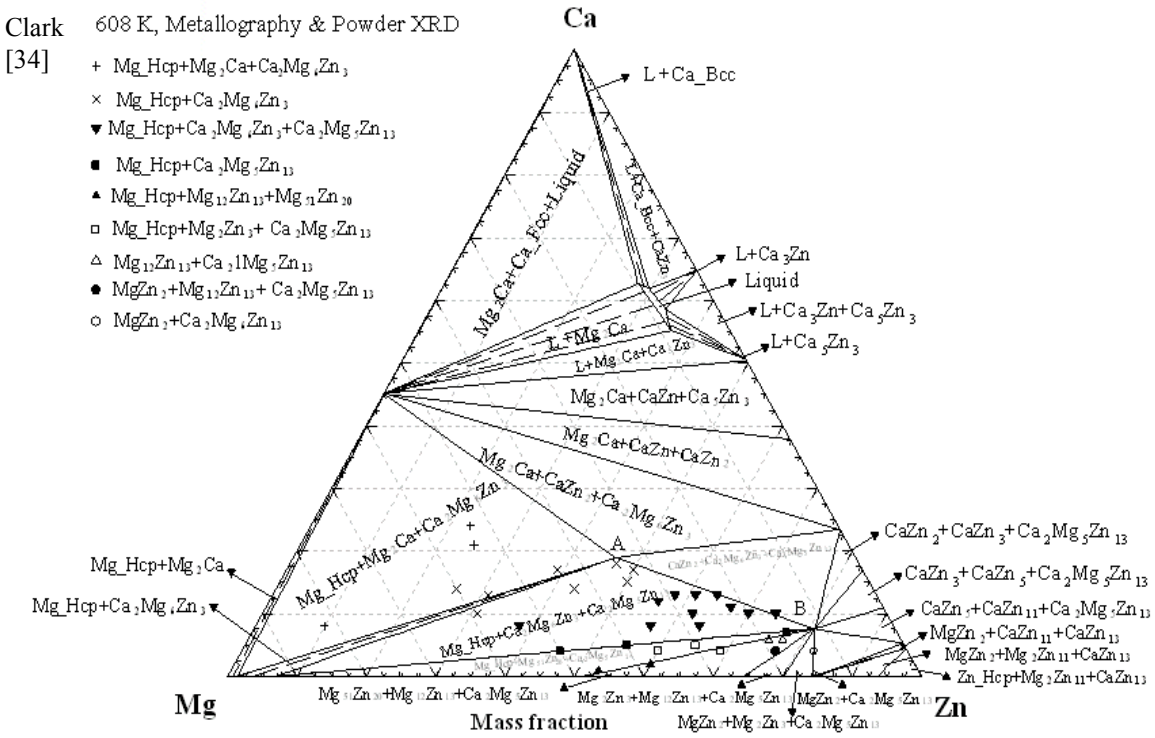

Fig 1.2: Calculated isothermal section of the Ca-Mg-Zn system at 335ºC [12].

Despite the fact that this system was studied many times in the past, there are still several contradictory results need to be verified. The details will be shown in the next chapter. Hence, the research in this thesis is directed towards resolving these contradictions by experimentally investigating the Ca-Mg-Zn system via diffusion couples and key experiments.

Objectives of the present work

The main purpose of adding alloying elements to pure magnesium is to increase its strength, to improve its corrosion and creep resistance which is important for commercial applications including those in automotive and aerospace industries. Since the Ca-Mg-Zn

system is promising as a next-generation material in both transportation and biomedical applications, understanding the phase diagram and the crystal structure of the ternary compounds in this system significant. The present work aims at:

- Studying the phase relations and solubility limits of binary and ternary compounds using SEM, EPMA and X-ray diffraction techniques.
- Determination of the crystal structures of the ternary compounds using EBSD, TEM and X-ray diffraction techniques.
- Studying the morphologies of diffusion couples in the Ca-Mg-Zn phase diagram at 335ºC and establishing the mechanism of these morphologies.
- Construction of the isothermal section of Ca-Mg-Zn phase diagram at 335ºC experimentally.

CHAPTER 2

Literature review

2.1 Ternary phase diagram

The initial experimental work on the Ca-Mg-Zn phase diagram was carried out in 1934 by Paris [14]. Based on thermal analysis and metallography, he reported one ternary compound with the $Ca_2Mg_5Zn_5$ composition, as shown in Fig 2.1, whose crystallographic information and other thermophysical properties could not be found in the literature.

The isothermal section in the Mg-Zn side of the Ca-Mg-Zn system at 335ºC was studied by Clark [15] using metallography and powder X-ray diffraction. He [15] reported two solid solutions β and ω as shown in Fig 2.1. These are different from the composition of $Ca_2Mg_5Zn_5$ reported by Paris [14]. The compositions of the two ternary compounds and XRD patterns were mentioned by Clark later in the publication of the Joint Committee on Powder Diffraction Standards (JCPDS) [16, 17] as $Ca_2Mg_6Zn_3$ and $Ca_2Mg_5Zn_{13}$. Both XRD patterns of the ternary phases were reported. The composition of $Ca_2Mg_6Zn_3$ is slightly different from his previous report [15] as β with extensive solubility range, but the composition of $Ca_2Mg_5Zn_{13}$ is consistent with ω. Then, Larinova et al. [18] worked on this system using XRD and reported a ternary compound with $Ca_2Mg_6Zn_3$ composition. Clark [16] and Larinova et al. [18] mentioned that this compound has a hexagonal structure with lattice parameters a = 9.725 Å, c = 10.148 Å, but did not report the space group or structure type.

Later, Jardim et al. [19, 20] worked on this system using Scanning Transmission Electron Microscopy (STEM) with Energy Dispersive X-ray Spectroscopy (EDS) as well as XRD. Several Mg-rich alloys were prepared in the form of ribbons using melt spinning technique. They claimed that all the observed precipitates belong to the same ternary compound $Ca_2Mg_6Zn_3$. Then, Oh-ishi et al. [21] investigated the same alloys by mould casting followed by TEM. Both of them reported a ternary compound with $Ca_2Mg_6Zn_3$ composition, which is similar to the compound given in the JCPDS card reported by Clark [16]. However, they reported this compound as a trigonal structure with space group $P\bar{3}1c$, lattice parameters a = 9.7 Å, c = 10 Å, and $Si_2Te_6Mn_3$ prototype, which does not agree with the hexagonal structure reported by Clark [16] and Larinova et al. [18].

In order to resolve these controversies [15, 16, 18-21] of both composition and crystallography, the solubility range and crystal structure of this compound $Ca_2Mg_6Zn_3$ are verified and investigated here. In addition, although the homogeneity range and XRD pattern of the other ternary compound $Ca_2Mg_5Zn_{13}$ were reported by Clark [15, 17], the crystal structure, including the space group, structure type and lattice parameters are not mentioned in the literature. Also, the ternary element solubility in the binary compounds has not been reported before. All of the above issues in this Ca-Mg-Zn system will be address in this thesis.

Brubaker and Liu [22], and Wasiur-Rahman and Medraj [12] modeled the Ca-Mg-Zn ternary phase diagram and included two ternary compounds. They did not consider the

ternary homogeneity ranges. The thermodynamic model proposed by Brubaker and Liu [22] was based on the random mixing of atoms in the liquid phase, which cannot properly handle the presence of short-range ordering. This system was remodeled using the modified quasichemical model by Wasiur-Rahman and Medraj [12]. The isotherm of Ca-Mg-Zn system at 335ºC is calculated in mole fraction based on the work of Wasiur-Rahman and Medraj [12], as shown in Fig 2.1. Since the contradictory results affect the accuracy of the thermodynamic model of this system, studing this system experimentally is significant.

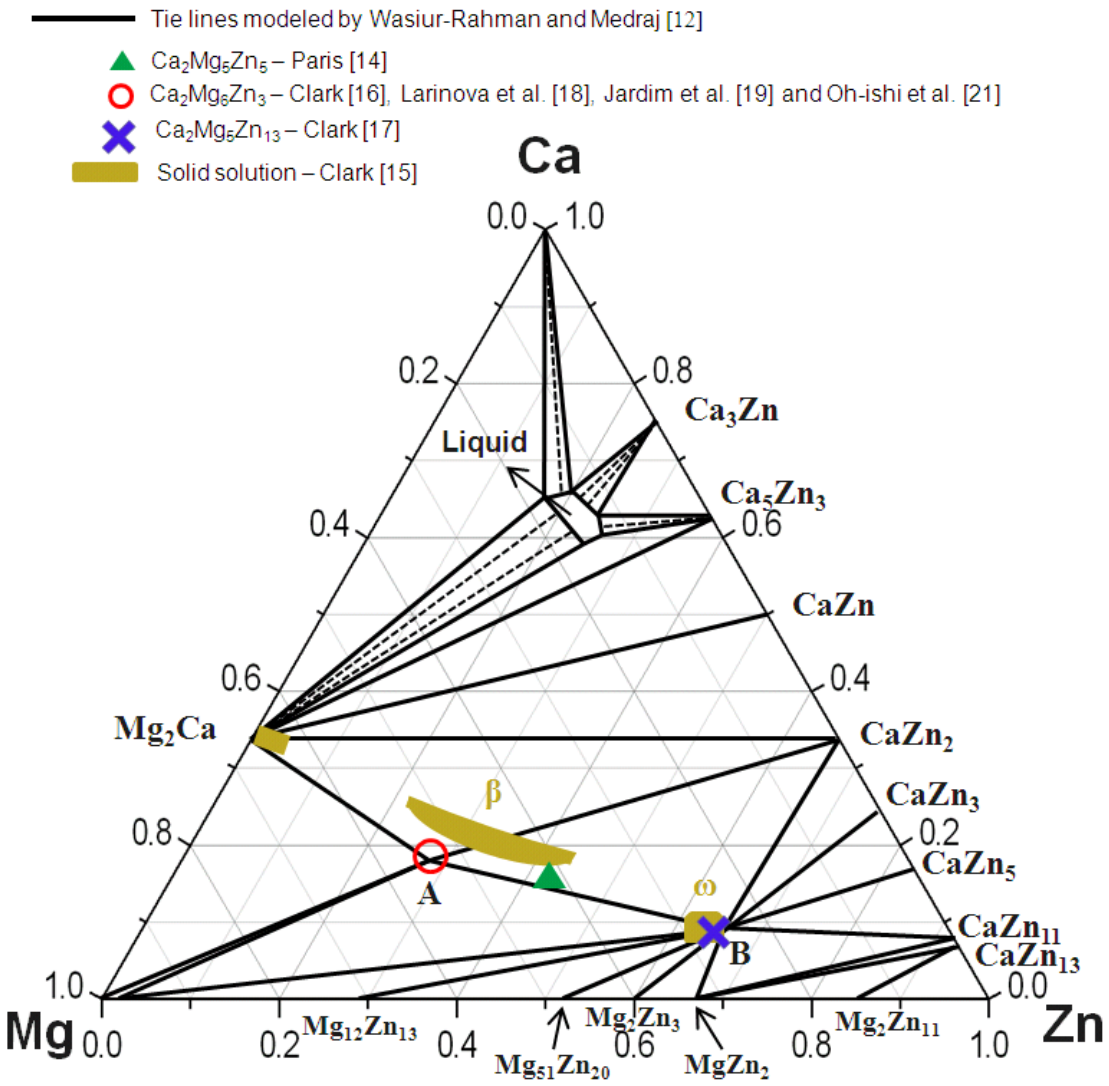

Fig 2.1: Isothermal section of the Ca-Mg-Zn system at 335ºC calculated based on the database of Wasiur-Rahman and Medraj [12] including comparison of the ternary compounds reported in the literature [14-19, 21].

2.2 Binary phase diagram

The most recent descriptions of the constituent binaries of the Ca-Mg-Zn system are discussed in the following sections.

2.2.1. Mg-Zn phase diagram

The equilibrium phases in the Mg-Zn system include liquid, Mg solid solution, $MgZn_2$ solid solution (C14), hexagonal Zn and other four stoichiometric compounds, as shown in Fig 2.2. The maximum solid solubility of Zn in Mg is 2.5 at.% Zn at 613 K.

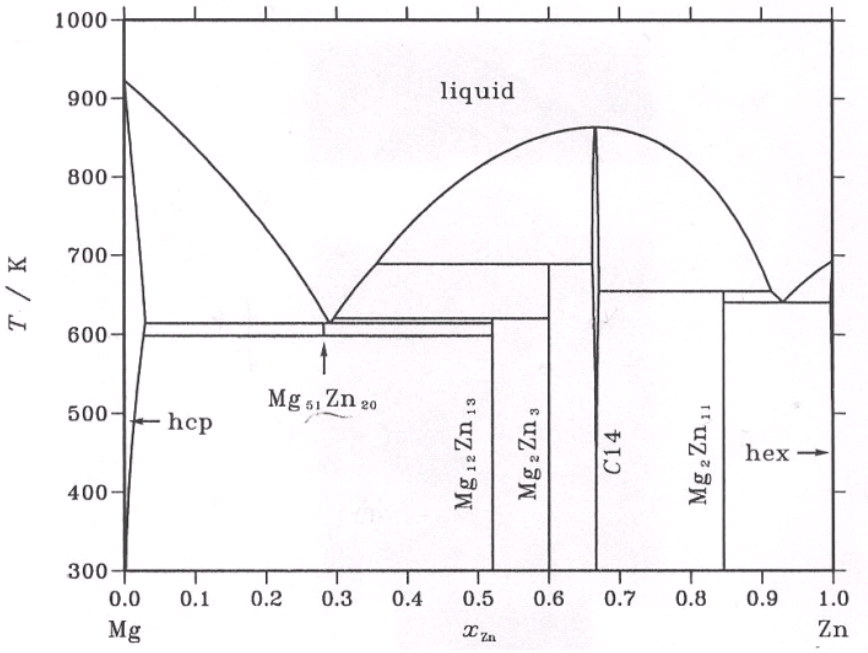

Fig 2.2: Mg-Zn binary phase diagram.

2.2.2. Ca-Zn phase diagram

The equilibrium phases of Mg-Zn system contain eight stoichiometric compounds as illustrated in Fig 2.3: Ca_3Zn, Ca_7Zn_4, CaZn, $CaZn_2$, Ca_7Zn_{20}, $CaZn_5$, $CaZn_{11}$ and $CaZn_{13}$. $CaZn_2$, $CaZn_5$ and $CaZn_{11}$ melt congruently and the other five compounds undergo peritectic decomposition.

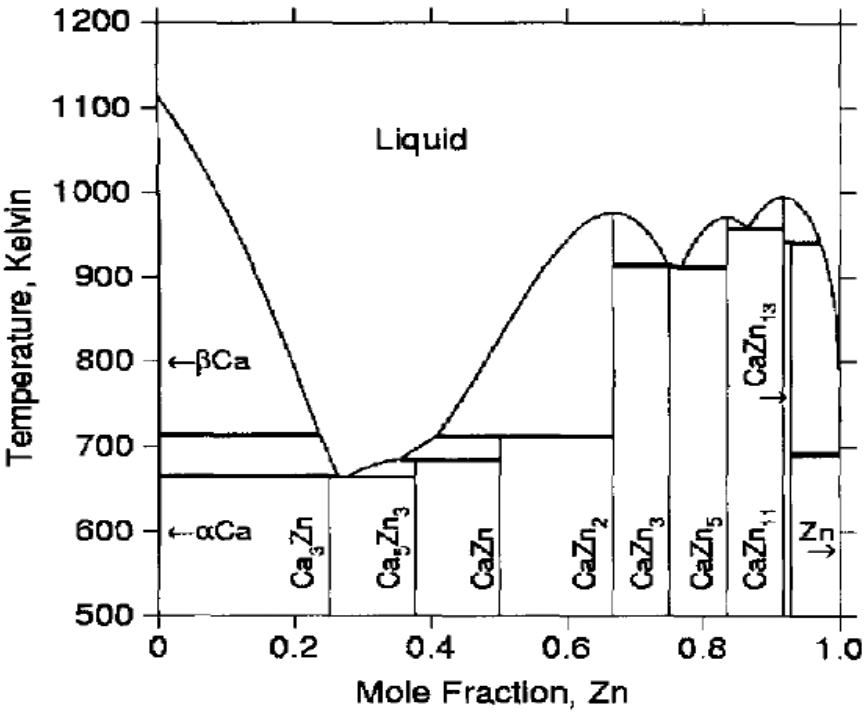

Fig 2.3: Ca-Zn binary phase diagram.

2.2.3. Ca-Mg phase diagram

The equilibrium phases of Mg-Zn system include the liquid, hcp-Mg, Mg_2Ca stoichiometric binary compound, bcc-Ca and fcc-Ca, as shown in Fig 2.4. The congruent melting intermediate compound Mg_2Ca has the Laves C14 crystal structure which is similar to $MgZn_2$.

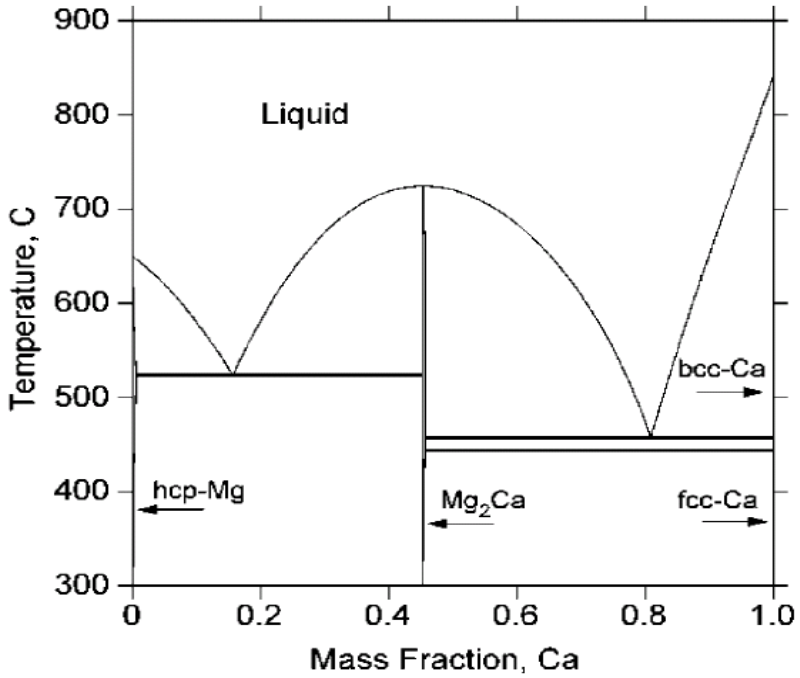

Fig 2.4: Ca-Mg binary phase diagram.

2.3 Diffusion couple approach

The present study employs the high throughput diffusion couple technique, a valuable experimental approach to map the phase diagram of ternary systems [23-27]. In the solid-solid diffusion couples or diffusion multiples, there are no problems associated with melting or powder contamination since all the phases form by diffusion reactions of bulk constituents at the temperature of interest [28]. Equilibrium phases form grain or layers and local equilibrium occur at the phase interface [28]. However, the diffusion couples approach is not omnipotent [28]. When they are used in determining phase diagrams, one should always be watchful for the possibility of missing phases [25, 28]. This may happen because the nucleation of these phases does not take place, or even if the nucleation occurs, the growth rate of these phases is too slow resulting in too thin diffusion layers to determine by EPMA. This can result in inaccuracies in estimating tie-

line compositions for these phases, because it is difficult to extrapolate to the interface based on a few data points. In order to solve this problem and to assure the consistency of the analysis, other diffusion couples with different terminal compositions should be used to compare and determine the phase equilibria. It is also important to verify whether the known binary and ternary phases form. Furthermore, in order to guarantee the precision and reliability of the information obtained, in this work, a combination of the diffusion couples technique with an investigation of selected equilibrated alloys is desirable, especially for the regions where the exact phase boundaries are questionable.

CHAPTER 3

Experimental procedures

In order to study the Ca-Mg-Zn ternary system, nine diffusion couples and 32 key alloys have been prepared to map the whole composition range at 335ºC based on the preliminary thermodynamic model of Wasiur-Rahman and Medraj [12]. The reason of choosing the annealing temperature as 335ºC:

- The annealing temperature should be as high as possible, because heat treatment, with higher annealing temperature, the interdiffusion and reaction among elements are easier to take place, also the alloys cause less time to achieve the equilibrium.
- The annealing temperature should be lower than the lowest point of liquidus curve, which is the Mg-rich eutectic at 341 ºC in the Mg-Zn system.

The starting materials are high-purity Mg ingot of 99.8%, Zn with purity of 99.99%, and Ca with 99%, all supplied by Alfa Aesar. The key alloys are prepared in an arc-melting furnace with water-cooled copper crucible under a protective argon atmosphere using a non-consumable tungsten electrode. Samples are re-melted five times to ensure homogeneity.

3.1 Solid-solid and solid-liquid diffusion couples

To prepare solid-solid diffusion couples, the contacting surfaces are grinded down to 1200 grit SiC paper and polished using 1μm water-based diamond suspension and 99% pure ethanol as lubricant. The two end members are carefully pressed and clamped using a steel ring, placed in a Ta container, and sealed in a quartz tube filled with argon. Since Mg and Ca are susceptible to oxygen and nitrogen contamination, it is critical to keep the samples free from external interstitials by the quartz tube. The encapsulated samples are then annealed at 335ºC for 4 weeks followed by quenching in water. Terminal compositions of the solid-solid diffusion couples are shown in Fig 3.1 (a). Their compositions are as follows:

- DC1. $Ca_{17.6}Mg_{10.1}Zn_{72.3}$-Zn
- DC2. $Ca_{31.8}Mg_{17.5}Zn_{50.7}$-Zn
- DC3. $Ca_{31.7}Mg_{29.2}Zn_{39.1}$-Zn
- DC4. $Ca_{20.2}Mg_{63.1}Zn_{16.7}$-Zn
- DC5. $Ca_{10.3}Mg_{41.4}Zn_{48.3}$-Zn
- DC6. $Ca_{9.8}Mg_{74.7}Zn_{15.5}$-Zn

When the solid-solid diffusion couples failed, solid-liquid diffusion couples are used instead. The block of alloy with the lower melting temperature was melted on top of the block with higher melting temperature in the arc-melting furnace under a protective Ar atmosphere. The prepared samples were annealed at 335ºC for 4 weeks. Terminal compositions of the solid-liquid diffusion couples are illustrated in Fig 3.1 (b). Their compositions are as follows:

- DC7. Mg_2Ca-Zn
- DC8. Mg-$CaZn_2$

- DC9. $Mg_{69.4}Ca_{20.3}Zn_{10.3}$-$Mg_{22.3}Ca_{14.3}Zn_{63.4}$

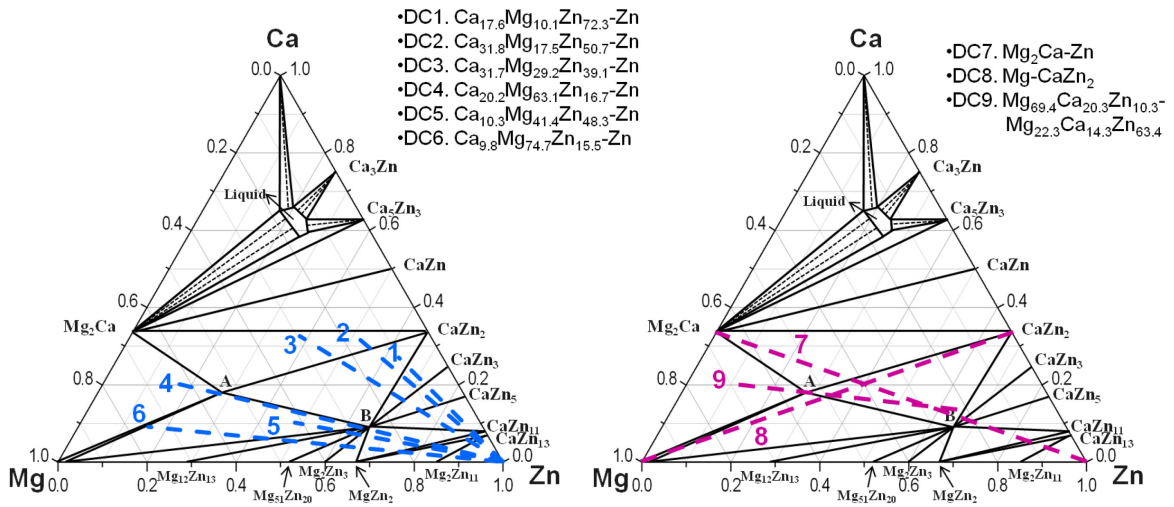

(a) (b)

Fig 3.1: Terminal compositions of the diffusion couples superimposed on the 335ºC calculated isothermal section of the Ca-Mg-Zn system based on the thermodynamic modeling [12]: (a) six solid-solid diffusion couples; (b) three solid-liquid diffusion couples.

3.2 Preparation of key samples

Key samples are prepared using the arc-melting furnace. They are encapsulated in tantalum foil, sealed in quartz tube under Ar atmosphere, annealed at 335ºC for 4 weeks, and quenched in water. The actual composition of the samples is determined by Inductively Coupled Plasma-Mass Spectrometry (ICP-MS). The difference between nominal compositions and actual compositions is below 3 at.% in most cases.

3.3 Characterization of samples

Diffusion couples and key samples have been experimentally investigated using SEM (Scanning Electron Microscopy), Electron Probe Microanalysis (EPMA) with Wavelength Dispersive X-Ray Spectrometry (WDS), Electron Backscattered Diffraction (EBSD), X-ray Diffraction (XRD) as well as Transmission Electron Microscopy (TEM). The microstructure, layer thickness, phase composition, and homogeneity ranges are analyzed using quantitative EPMA (JEOL-JXA-8900) with a 2μm probe diameter, 15kV accelerating voltage, 20nA probe current. Phi-Rho-Z (PRZ) matrix corrections (modified ZAF) are applied during the analysis. The error of the EPMA measurements is estimated to be about ±2 at.%. This value is obtained using statistical analysis of the compositions of selected phases from several samples. The phase composition measurements are performed perpendicular to the interfaces between every two adjacent phases in the diffusion couples. The equilibrium compositions of each phase are obtained by extrapolating the composition-distance curves for each element to the phase boundaries [25, 29].

X-ray diffraction is used for phase analysis and determination of the solubility limits in the key alloys. The XRD patterns are obtained using PANanalytical Xpert Pro powder X-ray diffractometer with a CuKα radiation at 45kV and 40mA. The XRD spectrum is acquired from 20 to 120º 2θ with a 0.02º step size. X-ray diffraction study of the samples is carried out using X'Pert HighScore Plus Rietveld analysis software in combination with Pearson's crystal database [30].

In order to improve surface preparation for EBSD diffraction, the samples are prepared using first standard mechanical metallographic preparation, then a plasma cleaning, and optimized ion milling, finally cleaning with plasma again. Three successive stages of ion milling are used on the surface of the diffusion couples with a current of 5mA and accelerated voltages of 3.5kV for 2hr, 2.5kV for 30min and 1.5kV for 30min. As a very powerful and efficient technique for crystal structure identification with a high spatial resolution [31], EBSD analysis is performed using a Hitachi SU-70 Schottky-SEM equipped with a Nordlys F+ camera and OXFORD HKL CHANNEL 5 software. Typical operation parameters are 20kV accelerating voltage and 13nA beam current. Secondary Electron Images (SEI) are employed for the observation of surface topographic features. Phase identification has been accomplished by a direct match and indexation of the Kikuchi diffraction bands with simulated diffraction patterns generated by means of known structure types and lattice parameters.

Focused Ion Beam (FIB) is used to lift a specimen of the ternary compound from key sample ($Ca_{18.0}Mg_{44.2}Zn_{37.8}$) and to obtain the crystallographic information using TEM. The Selected Area Electron Diffraction (SAED) and CM20 FEG TEM operated at 200kV are used to analyze this ternary compound. Ternary key sample $Ca_{6.2}Mg_{48.3}Zn_{45.5}$ is prepared to study the crystallographic information of IM3 compound and phase relations between IM3 and Mg solid solution. The sample is crushed using a mortar and pestle and the fragments are suspended in ethanol before depositing them on a carbon coated Cu grid. The Selected Area Electron Diffraction (SAED) and Philips CM200 TEM operated at 200kV are used to analyze the IM3 compound and Mg solid solution.

CHAPTER 4

Results and Discussions

4.1 Isothermal section at 335ºC through diffusion couples

4.1.1 Solid-solid diffusion couples

Backscattered electron images of the solid-solid DC1 with gradually increased magnification of the area of interest are illustrated in Fig 4.1 (a) and (b). During heat treatment, extensive interdiffusion among Ca, Mg and Zn took place allowing various equilibrium phases to form. EPMA line scan has been used to determine the solubility range of $CaZn_{11}$, $CaZn_{13}$, and Zn phases, as shown in Fig 4.1(a) and Fig 4.2. Spot analysis has been carried out for composition identification of smaller grains, such as those of $CaZn_5$ and IM2. Based on the compositional information obtained by EPMA analysis, ternary and binary intermetallic compounds and the solid solubility of the binary compounds extending in the ternary system have been identified. Using the local equilibrium at the interfaces formed between the phases, the sequence of the phases along the diffusion path is: $CaZn_2$ + (IM1) → $CaZn_2$ + IM2 → $CaZn_3$ + IM2 → $CaZn_5$ + IM2→ $CaZn_5$ + ($CaZn_{11}$) → ($CaZn_{11}$) → $CaZn_{13}$ → Zn. The following four phase triangulations are identified from Fig 4.1(b): $CaZn_2$, (IM1) and IM2; $CaZn_2$, IM2 and $CaZn_3$; $CaZn_3$, IM2 and $CaZn_5$; $CaZn_5$, IM2 and $CaZn_{11}$. Two ternary intermetallic compounds have been detected in this diffusion couple by EPMA spot analysis: ternary intermetallic 1 (IM1) with composition 16.7 at.% Ca, 26.0 at.% Mg, and 57.3 at.% Zn.

IM2 is a new ternary stoichiometric compound with $Ca_{14.4}Mg_{15.8}Zn_{69.8}$ composition. The result of the 80µm EPMA line scan of the diffusion couple is shown in Fig 4.2. The line scan clearly illustrates that the $CaZn_{11}$ phase forms substitutional solid solution where Mg substitutes Zn atoms while Ca content remains constant at 8.3 at.%. On the other hand, $CaZn_{13}$ does not show significant solid solubility. The least squares approximation is used to obtain the solubility limits of the $CaZn_{11}$ compound. The deviation from the linearity is about ±1 at.%, which is within the error limits of the EPMA measurements.

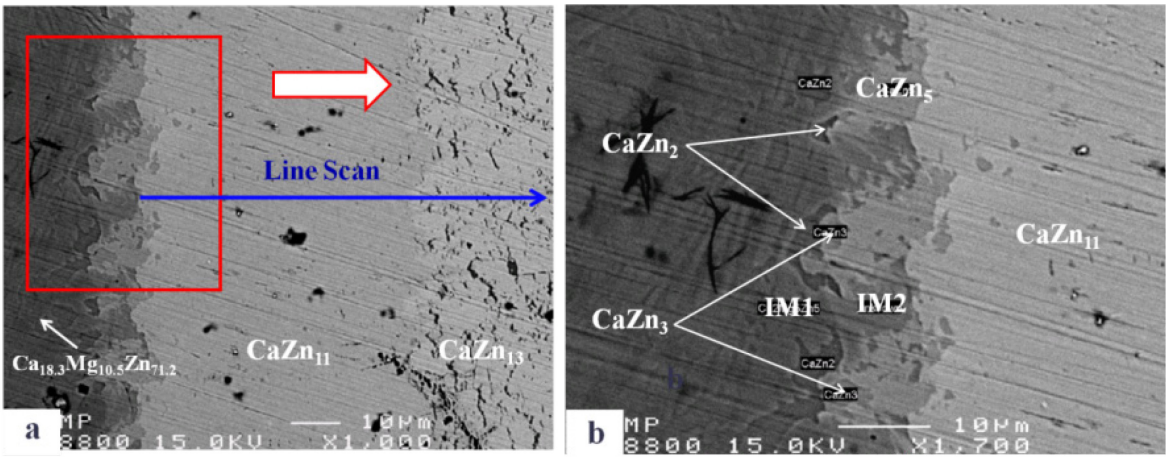

Fig 4.1: (a) and (b) Backscattered electron images of the solid-solid DC1 annealed at 335ºC for 4 weeks, showing the formation of seven different intermetallic compounds, with the tooth-like morphology clearly showing up.

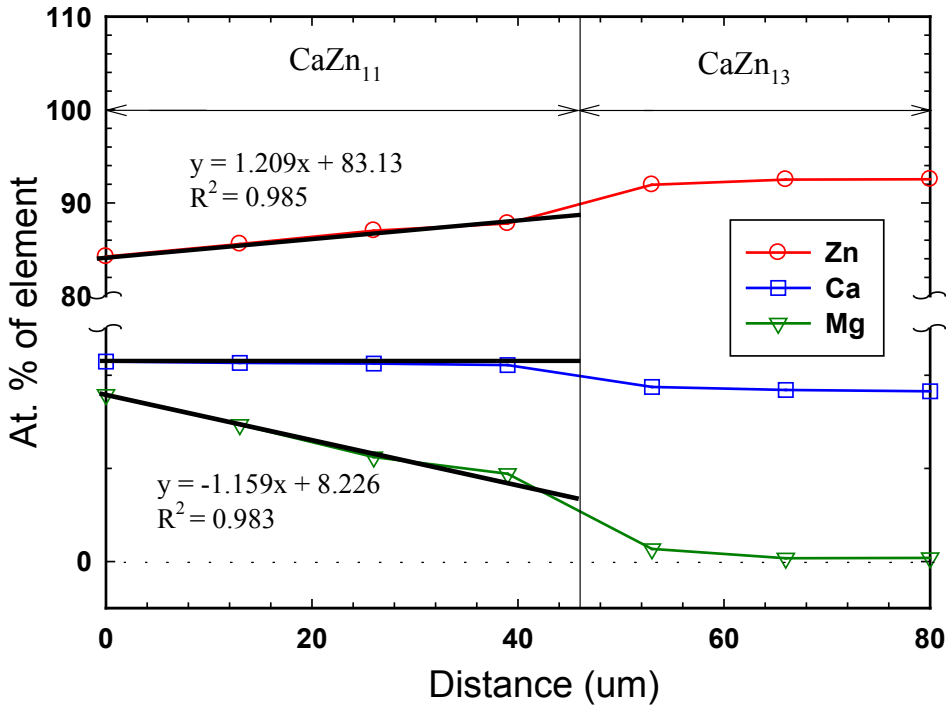

Fig 4.2: Composition profile of the line scan in Fig 4.1(a).

Backscattered electron images of the solid-state DC3 with increased magnification of the area of interest are illustrated in Fig 4.3. The sequence of the phases along the diffusion path is: Zn → Mg_2Zn_{11} → ($CaZn_{13}$) + Mg_2Zn_{11} → ($CaZn_{13}$) + ($MgZn_2$) → ($CaZn_{11}$) → IM2 → IM1 → $CaZn_2$ + (Mg_2Ca). The following two phase triangulations are identified from Fig 4.3: ($CaZn_{13}$), ($MgZn_2$) and Mg_2Zn_{11}; IM2, (Mg_2Ca) and $CaZn_2$. Two ternary intermetallic compounds have been observed in this diffusion couple by EPMA: ternary intermetallic 1 (IM1) with composition 16.7 at.% Ca, 25.4 at.% Mg, and 57.9 at.% Zn and ternary intermetallic 2 (IM2) which is a new ternary stoichiometric compound with $Ca_{14.4}Mg_{15.8}Zn_{69.8}$ composition. $CaZn_{11}$ and $CaZn_{13}$ compounds have been found to form extended substitutional solid solutions where Mg substitutes Zn up to 8.3 and 9.1 at.% Mg, respectively. The experimental results indicate that no significant solid solubility of

Mg_2Zn_{11}. Binary homogeneity range of the $MgZn_2$ isolated precipitates imbedded in the ($CaZn_{13}$) matrix is determined as 33.3 to 36.2 at.% Mg by EPMA point analysis and the result is consistent with the Mg-Zn binary phase diagram reported by Park and Wyman [32].

The morphology of the diffusion zone evolved in this solid-state DC3 has been studied. The Mg_2Zn_{11} diffusion layer appears as a continuous layer adjacent to the end member Zn, as demonstrated in Fig 4.3(a). Then the morphology changes to an interpenetrating type structure consisting of isolated ($MgZn_{11}$) precipitates and (3.8-6.4 at.% Mg)matrix ($CaZn_{13}$). After that, the morphology of the reaction layer changes gradually, another two two-phase structure consisting of the same matrix ($CaZn_{13}$) but with different Mg concentration (6.4-9.1 at.% Mg) and the isolated precipitates of $MgZn_2$ compound form. Then the $CaZn_{11}$ diffusion layer appears as a continuous layer changing to the IM2 compound and gradually transforming into (IM1), as illustrated in Fig 4.3(b). Then the morphology terminates at the two-phase end member (Mg_2Ca) and $CaZn_2$ alloy.

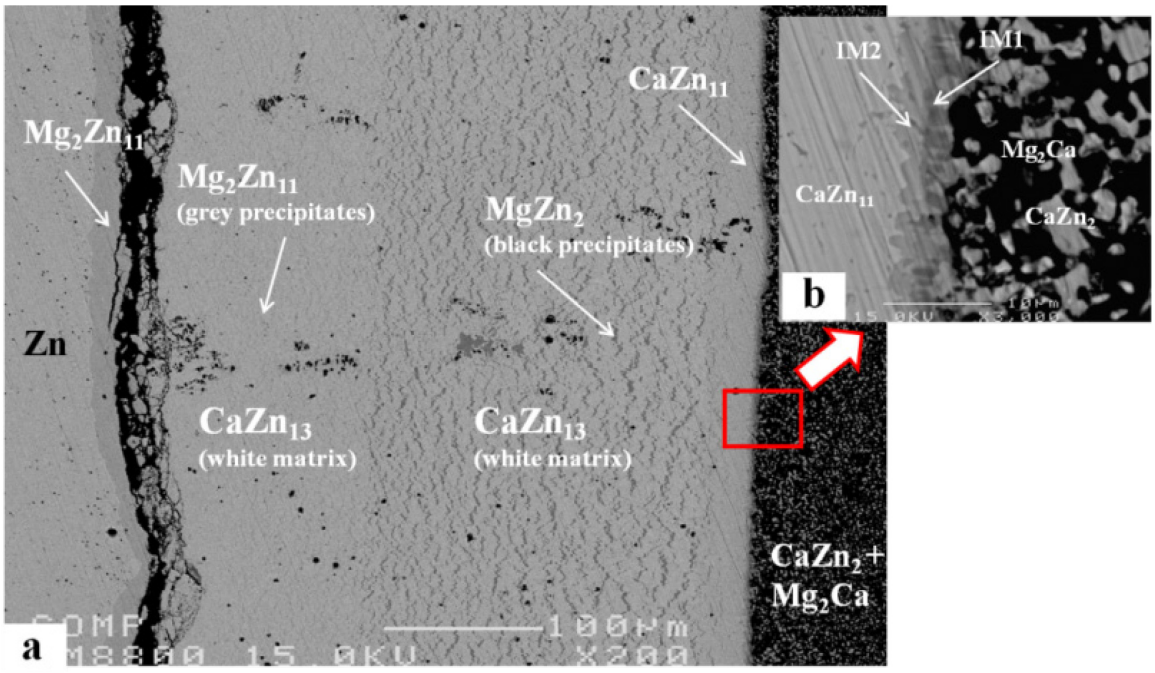

Fig 4.3: (a) and (b) Backscattered electron images of the solid-state DC3 annealed at 335ºC for 4 weeks, showing the formation of eight different intermetallic compounds.

Combining the EPMA results of the solid-solid DC1, DC2 and DC3, a large amount of phase equilibrium information has been obtained. A partial isothermal section at 335ºC of the Ca-Mg-Zn system has been constructed and the phase relations are demonstrated in Fig 4.4. The existence of (IM1) and IM2 ternary compounds has been confirmed by these three diffusion couples. The (IM1) substitutional solid solution has been determined and IM2 is considered to be a stoichiometric compound. Based on EPMA analysis, the solid solubility limit of Mg_2Ca compound has been determined as 31.3 at.% Ca, 63.5 at.% Mg and 5.2 at.% Zn, where Zn atoms substitute both Ca and Mg atoms, which is consistent with the extended solid solution of Mg_2Ca phase reported by Clark [15]. $CaZn_{11}$ and $CaZn_{13}$ compounds have been found to form extended substitutional solid solutions where Mg substitutes Zn up to 8.35 and 9.80 at.% Mg, respectively. Binary homogeneity range of $MgZn_2$ isolated precipitates imbedded in the ($CaZn_{13}$) matrix is determined as

33.3 to 36.2 at.% Mg by EPMA point analysis. This result is consistent with the Mg-Zn binary phase diagram reported by Park and Wyman [32].

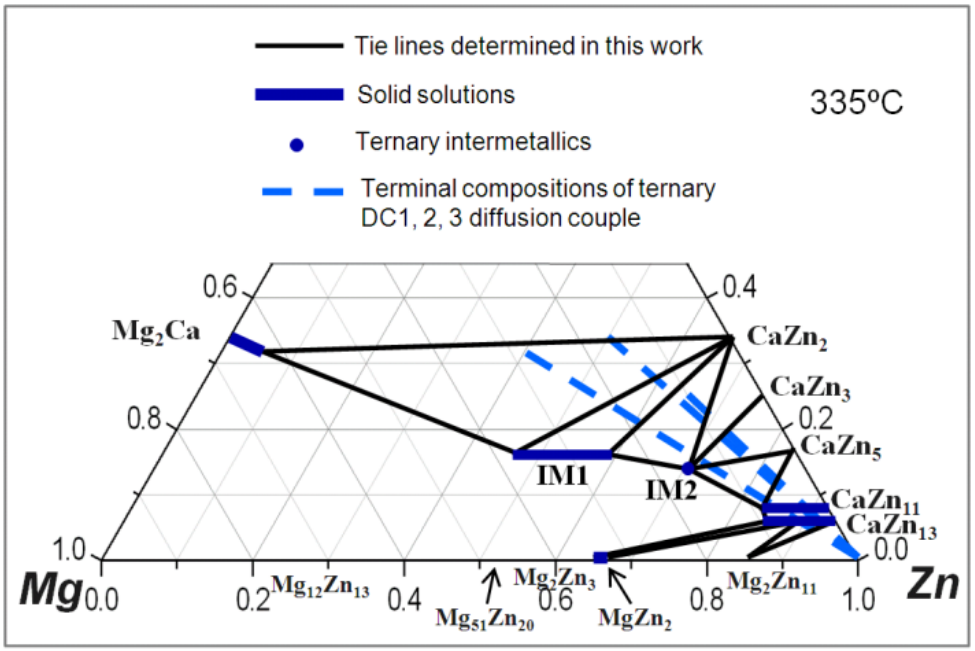

Fig 4.4: Partial isothermal section of the Ca-Mg-Zn system obtained from solid-solid DC1, DC2 and DC3 annealed at 335ºC for 4 weeks.

Backscattered electron images of the solid-solid DC4 diffusion couple annealed at 335ºC for 4 weeks are shown in Fig 4.5. The result of the EPMA 140µm line scan of the diffusion couple is shown in Fig 4.6. Two phases are identified by EPMA line scan: $Ca_2Mg_5Zn_{13}$ (IM3), and IM1 solid solution. The line scan clearly demonstrates that the IM1 compound forms substitutional solid solution where Mg substitutes Zn atoms while Ca content remains constant at 16.7 at.%. The least squares approximation was used to establish the concentration profiles of this compound. The change of Mg and Zn concentration profiles show that the substitution of Zn by Mg has a linear relationship with the diffusion distance. The deviation from the linearity is ±2 at.% which is within the error limits of the EPMA measurement. The least squares approximation of the Ca

profile shows no changes in its concentration. Based on this diffusion couple, the tentative minimum and maximum solid solubility limits of the IM1 ternary compound determined by EPMA are 35.31 at.% Mg and 65.20 at.% Mg, respectively. Because the solubility limits can be identified by the triangulations between each phase, taking into account that the diffusion layers contacting IM1 compound in the diffusion couple do not correspond to the three phase field, it is possible that IM1 compound did not establish the maximum solubility range. Therefore, key samples are used to obtain the actual boundaries of this solubility range. The solid solubility of IM3 compound will be discussed in next section.

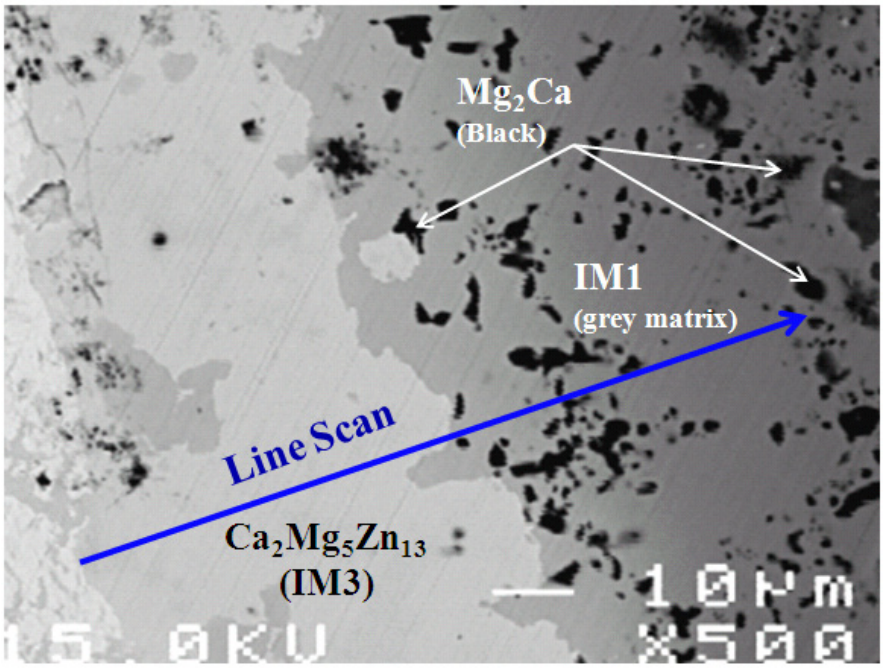

Fig 4.5: Backscattered electron images of the solid-solid DC4 annealed at 335ºC for 4 weeks.

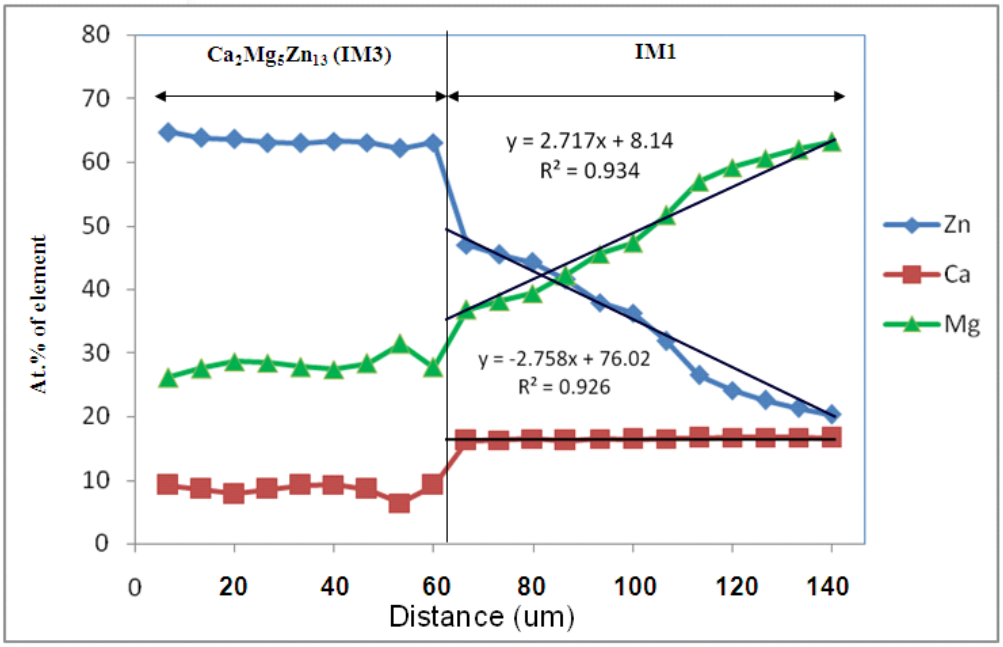

Fig 4.6: Composition profiles of the line scan shown in Fig 4.5.

Backscattered electron images of the solid-solid DC5, Fig 4.7 shows the formation of five different intermetallic compounds. Two ternary intermetallic compounds IM1 (hP36), IM3 (hP92) and the extended solid solubility of $CaZn_{13}$ (cF112) in the ternary system have been confirmed by both EPMA and EBSD. The crystal structure determination by EBSD is extremely useful for analyzing this system near the Zn-rich corner since several compounds have compositions very close to one another and EPMA data alone would not be enough to distinguish them. For instance, the extended binary homogeneity limits of $Ca(Mg,Zn)_{11}$ (8.3 at.% of Ca content) and $Ca(Mg,Zn)_{13}$ (7.1 at.% of Ca content) are very close to each other. Also, due to the extensive amount of Mg concentration (15.8 at.%) in the case of $Ca(Mg,Zn)_{13}$ compound, it is very difficult to conclude whether this is an isolated ternary compound or a binary compound with extended solubility in the ternary system. Fortunately, this confusion is resolved by EBSD crystal structure determination. Without EBSD, this would require the time-consuming FIB-TEM and selected area

electron diffraction analysis to confirm the results. The crystallographic information of intermetallic compound has been used for indexation of Kikuchi diffraction bands, as listed in Table 4.1. Detailed description of the crystal structure of IM1 ternary compound will be discussed in section 4.3.1. The EBSD patterns of IM1, IM3 and $CaZn_{13}$ are illustrated in Fig 4.8. The solubility limits of $CaZn_{13}$ compound extending in the ternary system has been analyzed by quantitative EPMA and the crystal structure of this compound has been confirmed by EBSD across the solubility line, as shown in Fig 4.7 and Fig 4.8. Besides, qualitative SEM/EDS mapping clearly demonstrates that the $CaZn_{13}$ compound forms substitutional solid solution where Zn substitutes Mg atoms while Ca content remains constant, as illustrated in Fig 4.9.

Analysis of the diffusion reaction zone reveals that the sequence of the phases along the diffusion path is: (IM1) + (IM3) + (Mg) → $CaZn_2$ + IM2 → (IM3) + ($MgZn_2$) → ($CaZn_{13}$) + ($MgZn_2$) → ($CaZn_{13}$) + Mg_2Zn_{11} → Mg_2Zn_{11} → Zn. The following three phase triangulations are identified from Fig 4.7: (IM1), (IM3) and (Mg); (IM1), ($CaZn_{13}$) and ($MgZn_2$); ($CaZn_{13}$), ($MgZn_2$) and Mg_2Zn_{11}. IM3 ternary compound has a complex homogeneity range: 8.2-9.1 at.% Ca, 27.1-31.0 at.% Mg and 60.8-64.7 at.% Zn, where Zn atoms substitute both Ca and Mg atoms. This is in agreement with the solid solution ω reported by Clark [34]. The solubility of Zn in (Mg) has been measured to be 2.3 at.% Mg. EPMA results indicate that Mg_2Zn_{11} does not have extended solubility in the ternary diagram.

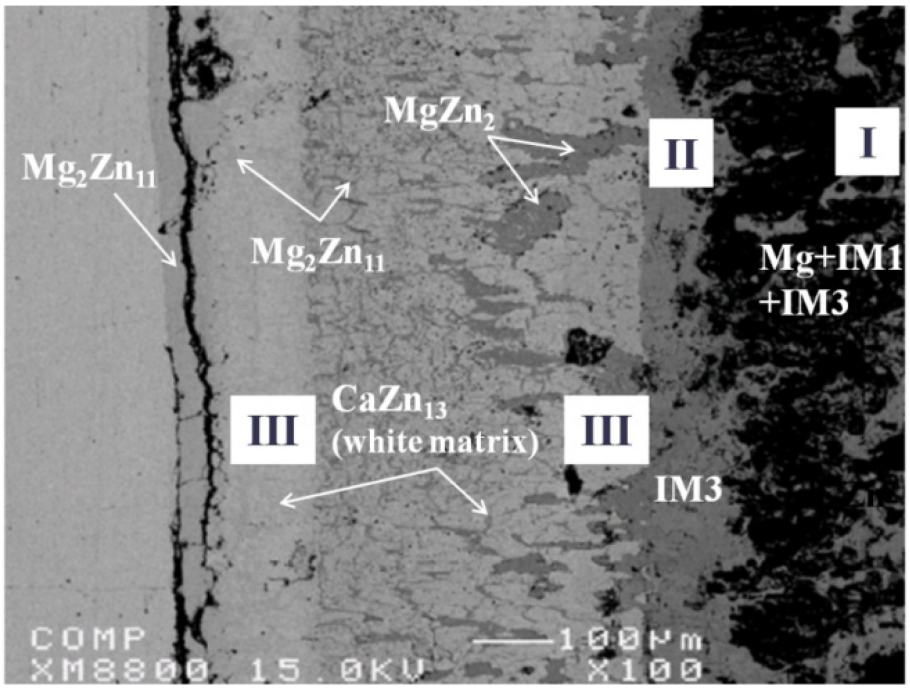

Fig 4.7: Backscattered electron images of the solid-solid DC5 annealed at 335ºC for 4 weeks showing the formation of six different intermetallic compounds.

Table 4.1: Crystallographic information of the phases in the Ca-Mg-Zn system [30].

Phase	Pearson symbol	Space group	Lattice parameters (Å)		
			a	*b*	*c*
$CaZn_2$	I12	*Imma* (74)	4.591	7.337	7.667
$CaZn_3$	hP32	*P6₃/mmc* (194)	9.168	9.168	7.327
$CaZn_5$	hP6	*P6/mmc* (191)	5.371	5.371	4.242
$CaZn_{11}$	tI48	*I4₁/amd O2* (141)	10.699	10.699	6.830
$CaZn_{13}$	cF112	*Fm-3c* (226)	12.154	12.154	12.154
Zn	hP2	*P6₃/mmc* (194)	2.665	2.665	4.947
Mg	hP2	*P6₃/mmc* (194)	3.199	3.199	5.154
$MgZn_2$	hP12	*P6₃/mmc* (194)	5.221	5.221	8.567
Mg_2Zn_{11}	cP39	*Pm-3* (200)	8.552	8.552	8.552
IM1	hP36	*P6₃/mmc* (194)	9.486	9.486	9.950
IM3	hP92	*P6₃/mmc* (194)	14.758	14.758	8.804

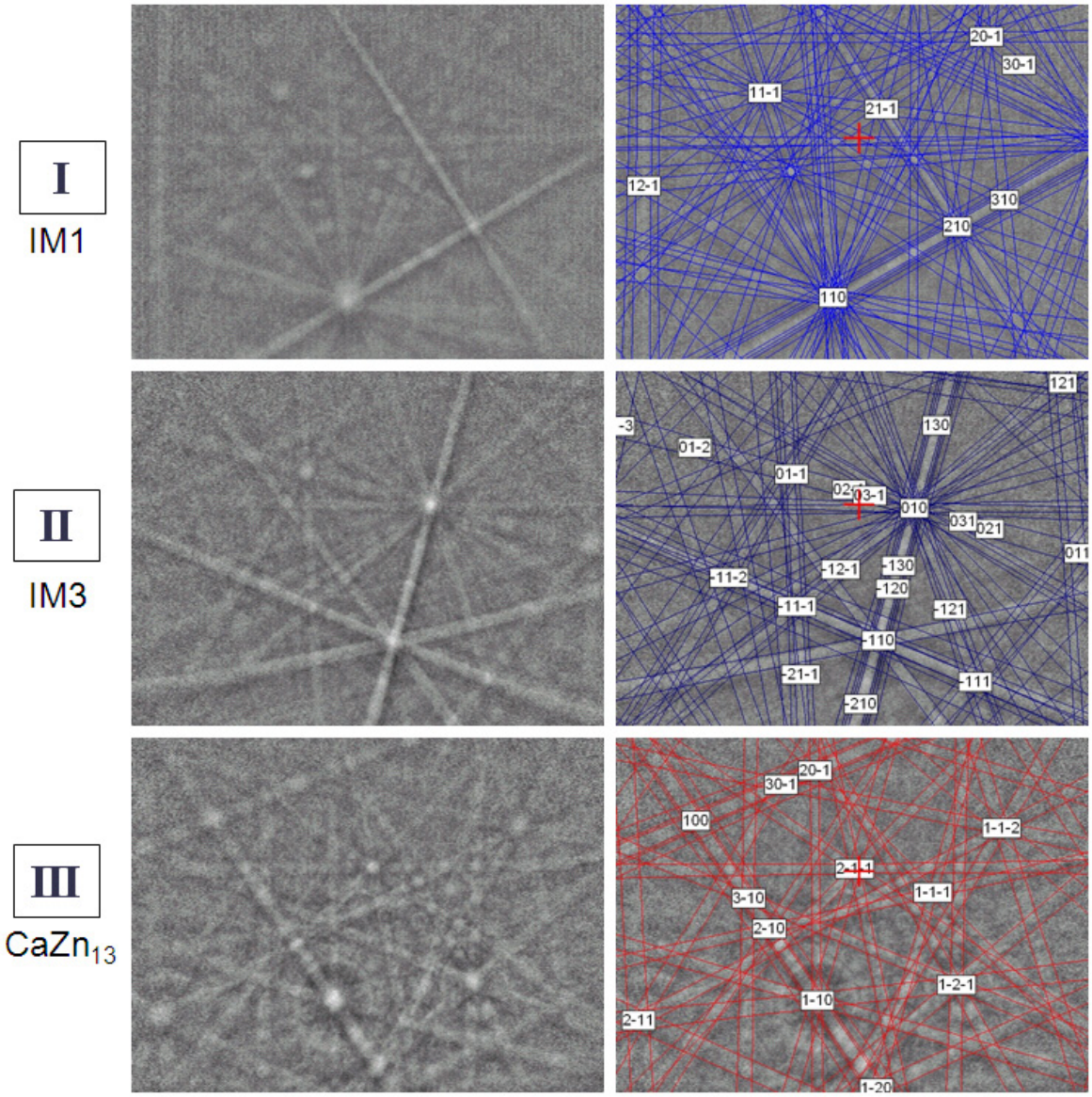

Fig 4.8: The EBSD pattern of (I) IM1, (II) IM3 ternary compounds and (III) $CaZn_{13}$ binary compound having an extended solid solubility in the ternary system. The un-indexed pattern is on the left and the indexed pattern is on the right.

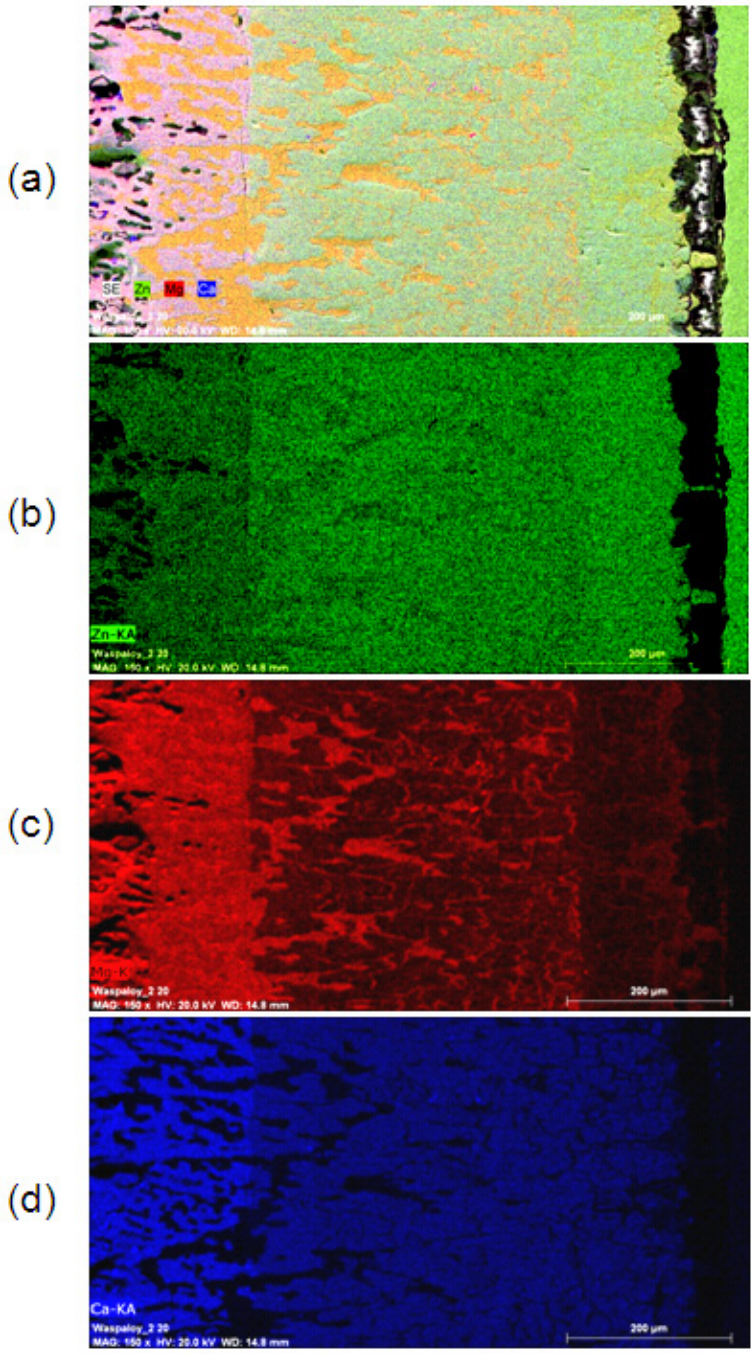

Fig 4.9: SEM/EDS mapping of solid-solid DC5, green, red and blue representing the Zn, Mg, Ca concentration profile, respectively.

Combining the EPMA results of the solid-solid DC4, DC5 and DC6, a partial isothermal section at 335ºC of the Ca-Mg-Zn system has been constructed and the phase relations are demonstrated in Fig 4.10. The IM1 substitutional solid solution has been studied. The existence of IM3 ternary phase has been confirmed by these three diffusion couples. IM3

compound forms a complex solid solution where Zn substitutes both Ca and Mg atoms. The maximum solid solubility of ($CaZn_{13}$) is determined as 15.5 at.% Mg.

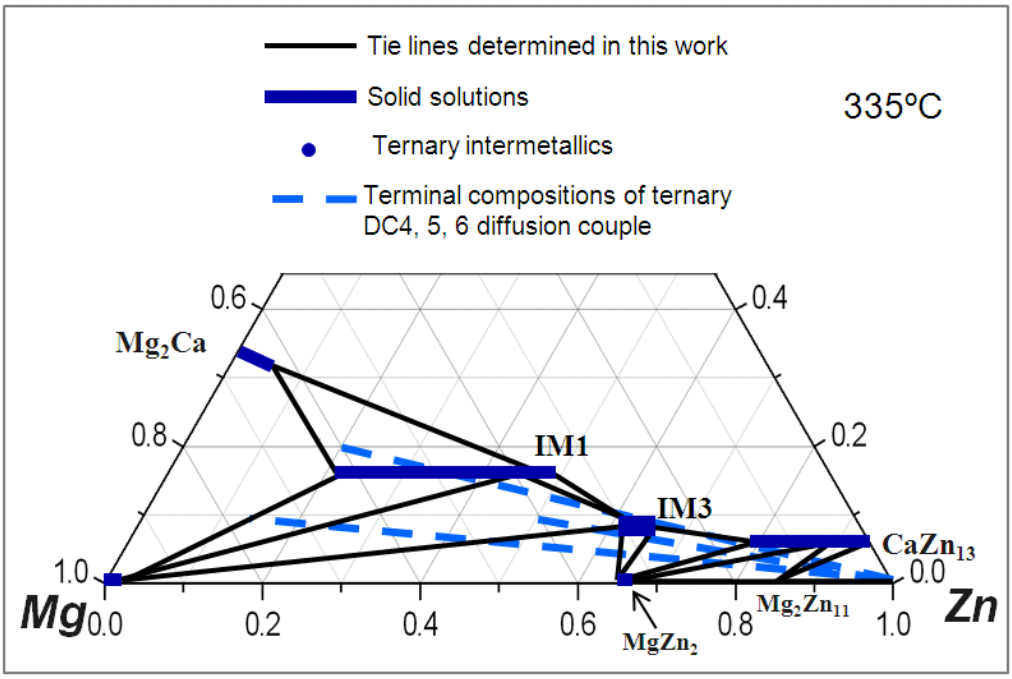

Fig 4.10: Partial isothermal section of the Mg-Zn-Ca system obtained from solid-solid DC4, DC5, DC6 annealed at 335ºC for 4 weeks.

4.1.2 Solid-liquid diffusion couples

Solid-liquid diffusion couples are used, when preparing solid-solid diffusion couples is impossible due to the brittleness of the end members. Mg_2Ca-Zn solid-liquid diffusion couple has been prepared and analyzed. Backscattered electron image of the solid-liquid DC7 annealed at 335ºC for 4 weeks, showing the formation of three different intermetallic compounds, is presented in Fig 4.11. Analysis of the diffusion reaction zone indicates that the sequence of the phases along the diffusion path is: (Mg_2Ca) → (IM1) → ($CaZn_{13}$) →Zn. The results of the 125µm EPMA line scan of the diffusion couple is shown in Fig 4.12 illustrating that the Mg_2Ca compound forms a complex solid solution

where Zn substitutes both Ca and Mg atoms. The IM1 and $CaZn_{13}$ compounds form substitutional solid solutions where Mg substitutes Zn atoms while Ca content remains constant at 16.7 and 7.3 at.%, respectively. The least squares approximation is used to establish the elemental concentration profiles of Mg_2Ca, IM1 and $CaZn_{13}$ compounds. Ca, Mg and Zn concentration profiles of Mg_2Ca show that the substitutions of Ca and Mg by Zn have linear relationships with the diffusion distance. Also, Mg and Zn concentration profiles of IM1 and $CaZn_{13}$ compounds show that the substitution of Mg by Zn has a linear relationship with the diffusion distance. The deviation from the linearity of all phases is ±2 at.%, which is within the error limits of the EPMA measurements. Based on this diffusion couple, the maximum solid solubility limit of the Mg_2Ca compound, determined by EPMA, is 31.1 at.% Ca, 64.1 at.% Mg and 4.8 at.% Zn, which is consistent with the solubility limits obtained from the solid-solid DC3 and DC4. The minimum and maximum solid solubility limits of the IM1 phase are 38.3 at.% Mg and 44.2 at.% Mg, respectively. The maximum solid solubility limits of the $CaZn_{13}$ compound is 12.1 at.% Mg.

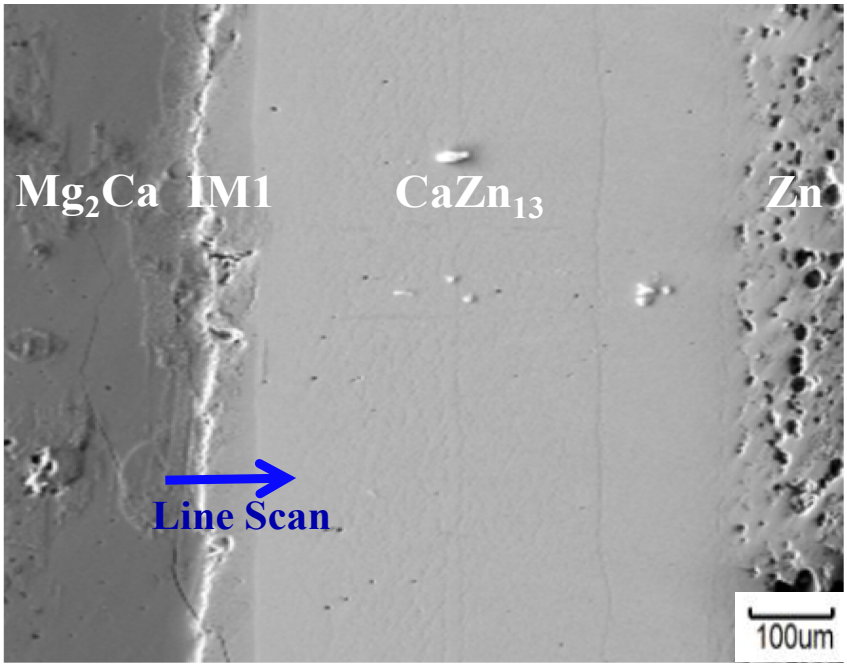

Fig 4.11: Backscattered electron image of the solid-liquid DC7 annealed at 335ºC for 4 weeks showing the formation of three different intermetallic compounds.

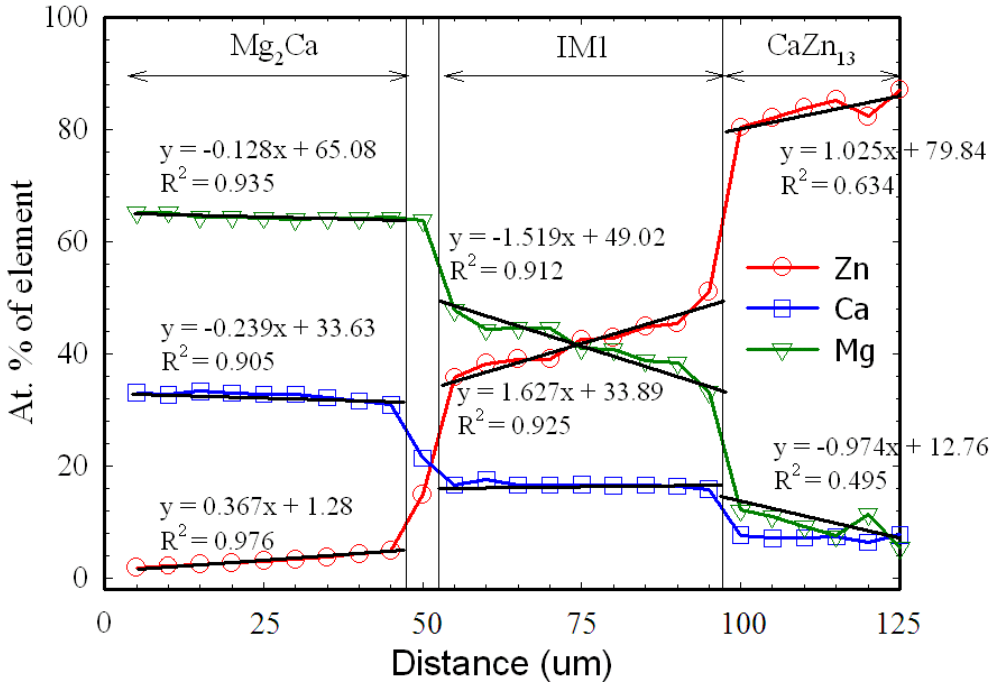

Fig 4.12: Composition profile of the line scan in Fig 4.11.

Combining the results obtained from six solid-solid diffusion couples and three additional solid-liquid diffusion couples, a partial isothermal section of the Ca-Mg-Zn system at 335ºC has been constructed and the phase relations are demonstrated in Fig 4.13. Besides, the experimental results revealed that the solid-liquid DC9 demonstrated tie lines among IM1, IM2, and IM3 compounds in the terminal alloy. This is contradictory to the results from solid-liquid DC7 which show that IM1 and $CaZn_3$ are in equilibrium. This situation is observed in other studies [33, 34] indicating that the local equilibrium at the interface is not real because the IM2 or IM3 is missing from between IM1 and ($CaZn_{13}$) due to their sluggish nucleation. In order to improve the reliability of the information obtained from the diffusion couples, 32 selected key alloys have been used to study the phase relations, phase boundaries and crystallographic information of the ternary compounds in the Ca-Mg-Zn system.

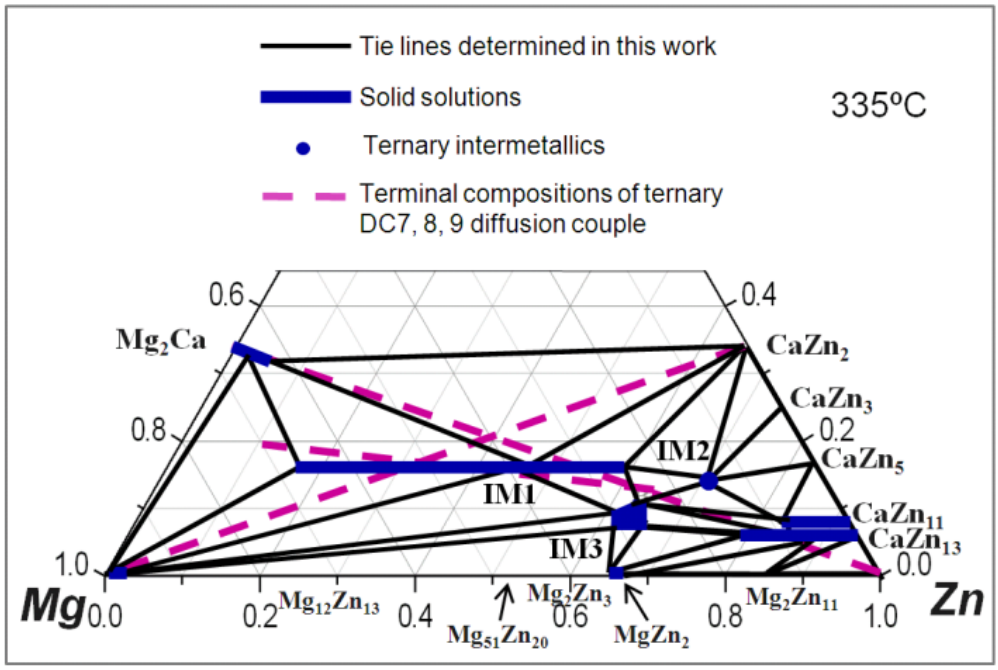

Fig 4.13: Partial isothermal section of the Mg-Zn-Ca system obtained from solid-liquid DC7, DC8 and DC9 annealed at 335ºC for 4 weeks.

4.2 Morphological evolution of the reaction zone in the diffusion couples

4.2.1 Solid-solid diffusion couples

In the solid-solid DC1, $CaZn_{11}$ and $CaZn_{13}$ phases are the dominant reaction products, as the microstructure in Fig 4.1(a) illustrates. Another morphology of the diffusion zone evolved in this diffusion couple is the 'tooth-like' structure, as can be seen clearly in Fig 4.1, which grows in a very irregular fashion, somewhat similar to the 'finger-like' structure that is reported in earlier works [24, 33, 34]. However, the concepts and mechanisms of the 'tooth-like' and 'finger-like' structures are different, as illustrated in Fig 4.14. In the present work, a two-phase terminal alloy $CaZn_2$ + (IM1) has been prepared. To understand the morphology of the 'tooth-like' structure model, a diffusion couple with 'finger-like' structure is used for comparison. The diffusion couple can be divided into several sub-diffusion couples. In this work, the DC1 with 'tooth-like' structure can be considered as several $CaZn_2$-$CaZn_{11}$ and IM1-$CaZn_{11}$ sub-diffusion couples. On one hand, the formation of $CaZn_5$, $CaZn_3$ phases is a result of the interdiffusion reaction between $CaZn_2$ and $CaZn_{11}$. On the other hand, IM2 ternary compound forms by the interdiffusion reaction between IM1 and $CaZn_{11}$, as illustrated with square marks in Fig 4.14(a). However, in the 'finger-like' structure, all the sub-diffusion couples present the phases formed by the same interdiffusion reaction. For example, NiSi and $NiSi_2$ phases form by the interdiffusion reaction between Ni_3Si_2 and Si.

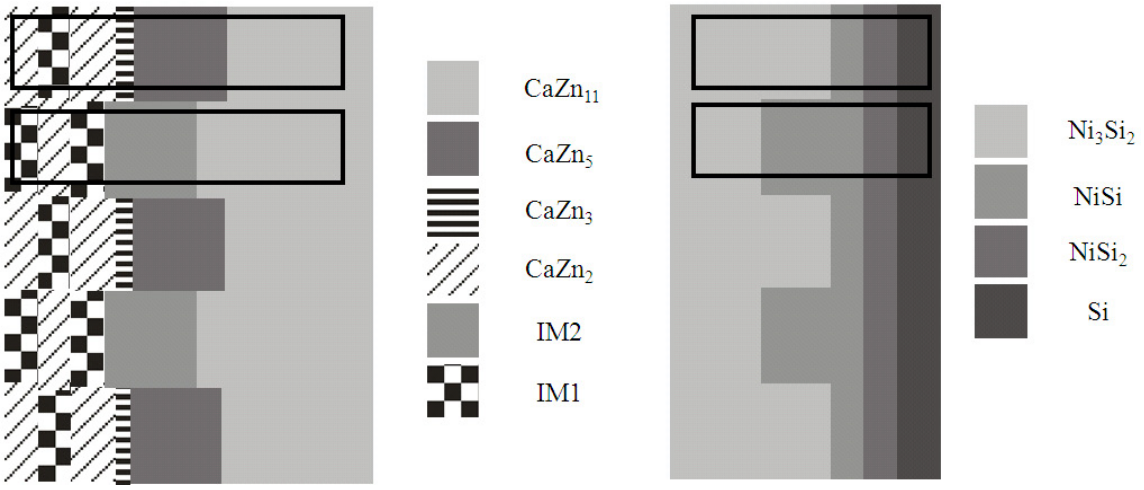

(a) (b)

Fig 4.14: Different morphologies of diffusion couple: (a) 'tooth-like' structure, (b) 'finger-like' structure.

The morphology of the diffusion zone evolved in the solid-solid DC5 is completely different from the morphology of solid-solid DC1. The diffusion reaction starts from the three-phase end member (IM1) + (IM3) + (Mg), as demonstrated in Fig 4.7, then the morphology changes to a single phase (IM3) layer. Afterwards, the morphology changes to isolated ($MgZn_2$) precipitates imbedded in the (IM3) matrix. Then, the matrix (IM3) changes to ($CaZn_{13}$) (6.4-15.5 at.% Mg) with the same isolated ($MgZn_2$) precipitates. After that, the morphology of the reaction layer changes gradually, another two-phase structure consisting of the same matrix ($CaZn_{13}$) but with different Mg concentration (3.8-6.4 at.% Mg) and the dendrite type structure of Mg_2Zn_{11} compound form. Then the Mg_2Zn_{11} diffusion layer appears as a continuous layer changing to the end member Zn. In order to calculate the interdiffusion coefficient, determination of the volume fraction of phases in the diffusion couple is needed. The volume fraction of the $MgZn_2$ precipitates with layer ($CaZn_{13}$) matrix is considerably higher than the layer ($CaZn_{13}$) with Mg_2Zn_{11} precipitates and the layer (IM3) with $MgZn_2$ precipitates, as illustrated in Fig 4.7. Furthermore, SEM/EDS elemental mapping has been carried out to study the evolution of

the morphology of this diffusion couple as shown in Fig 4.9. It also shows good consistency with the phase identification by EPMA. A schematic representation of the possible morphologies when a pure element is coupled with a three-phase alloy is depicted in Fig 4.15.

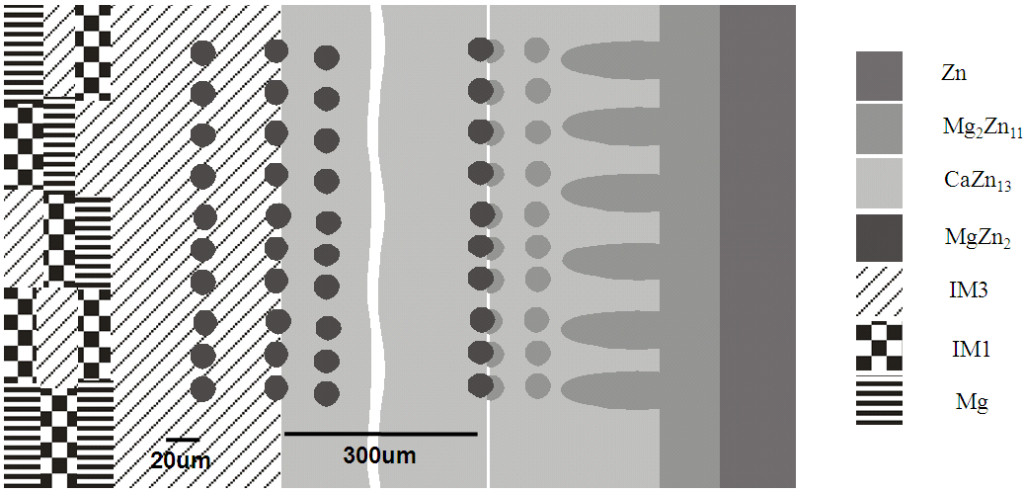

Fig 4.15: The possible morphologies in solid-solid diffusion couples when a pure element is attached to a three-phase alloy.

4.2.1 Solid-liquid diffusion couples

The morphology of the diffusion zone evolved in solid-liquid diffusion couples are different from those in solid-solid diffusion couples. For instance, in solid-liquid DC7, $CaZn_{13}$ phase is the dominant product during interdiffusion, as the microstructure in Fig 4.11 illustrates. Instead of forming 'tooth-like' morphology or matrix phase with isolated/dendritic type precipitates morphology, uniform layer morphology has occurred in this diffusion couple.

4.3 Key alloys

4.3.1 Solubility range and crystal structure of the IM1 ternary compound

4.3.1.1 Study of solubility range and crystal structure of IM1 compound via EPMA and XRD

Part of this work is directed towards determining the solubility range and the crystal structure of the Mg-rich IM1 ternary compound using 6 key samples (numbers 1 to 6), as illustrated in Fig 4.16. The composition and phase identification of these samples are summarized in Table 4.2. The actual chemical compositions of the alloys are measured by ICP and the composition of IM1 compound is determined by EPMA. The phase relations obtained from EPMA show great consistency with the results obtained by XRD. The XRD pattern of key sample 4 annealed at 335ºC for 4 weeks is shown in Fig 4.17(a). Full pattern refinement has been carried out by Rietveld method. The use of Si as an internal calibration standard enabled correcting the zero shift and specimen surface displacement which are the most serious systematic errors in x-ray powder diffraction patterns. The XRD pattern of sample 4 shows good consistency with that reported by Clark [16] as shown in Fig 4.17. The peak positions shift to higher angle with decreasing Mg content. The substitution of Mg by Zn, which has a smaller atomic radius, decreases the unit cell parameters. This is confirmed by the increase of the 2θ values of the peaks positions from sample 2 to 5 due to increasing Zn concentration, as demonstrated in Fig 4.18. Combining Pearson's crystallographic database [30] with Rietveld analysis, the crystal structure of IM1 compound has been found to have $Sc_3Ni_{11}Si_4$ prototype with hexagonal structure and *P6₃/mmc* (194) space group [35]. The XRD pattern generated

using $Sc_3Ni_{11}Si_4$ prototype [35] perfectly corresponds to the experimental patterns reported by Clark [16] and Larinova et al. [18]. However, this crystal structure contradicts with the trigonal structure reported by Jardim et al. [19] and Oh-ishia et al. [21]. Also the XRD pattern generated using $Si_2Te_6Mn_3$ prototype, reported by Jardim et al. [19] and Oh-ishia et al. [21] does not match with the current experimental results.

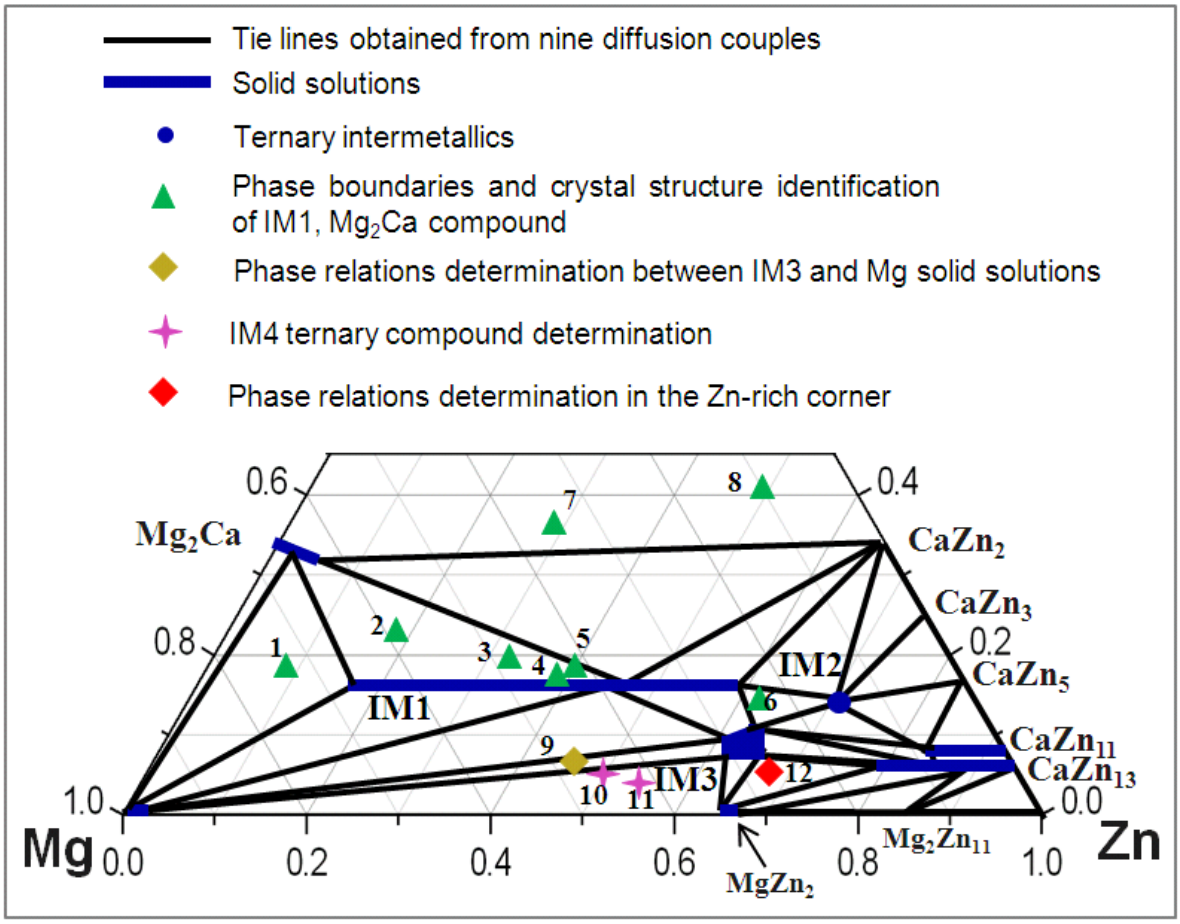

Fig 4.16: The actual composition of the key samples used to study the solubility ranges, phase relations and crystal structure of various compounds in the Ca-Mg-Zn system.

Table 4.2: The actual composition of the key samples and the phases present.

Sample No.	Actual composition identified by ICP (at.%)			Phases identification		Composition of IM1 identified by EPMA		
	Ca	Mg	Zn	By EPMA	By XRD	Ca	Mg	Zn
1	18.8	74.1	7.1	Mg	Mg	16.7	66.9	16.4
				Mg_2Ca	Mg_2Ca			
				IM1	IM1			
2	22.4	59.3	18.3	Mg_2Ca	Mg_2Ca	16.7	56.1	27.2
				IM1	IM1			
3	18.4	48.8	32.8	Mg_2Ca	Mg_2Ca	16.7	47.8	35.5
				IM1	IM1			
4	18.0	44.2	37.8	Mg_2Ca	Mg_2Ca	16.7	43.3	40.0
				IM1	IM1			
5	18.0	42.9	40.3	Mg_2Ca	Mg_2Ca	16.7	42.1	41.2
				IM1	IM1			
6	15.0	23.1	61.9	IM1	IM1	16.7	25.4	57.9
				IM3				
				IM2				

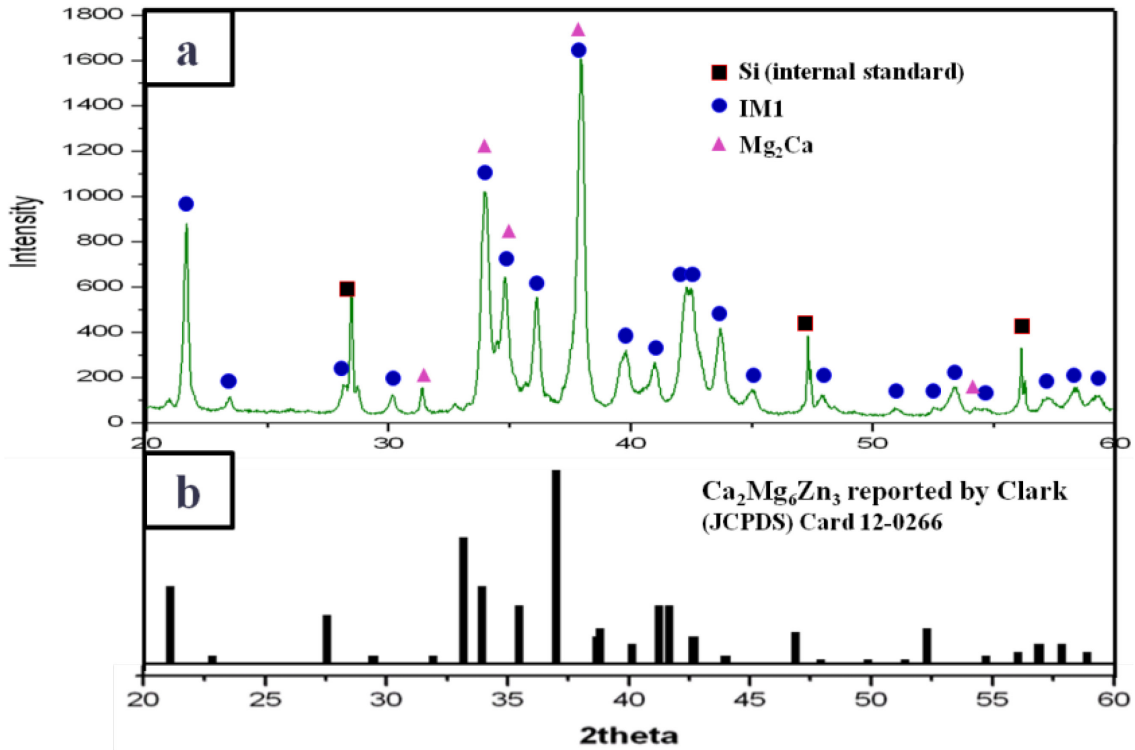

Fig 4.17: (a) XRD patterns of key samples 2; (b) XRD pattern reported by Clark [16].

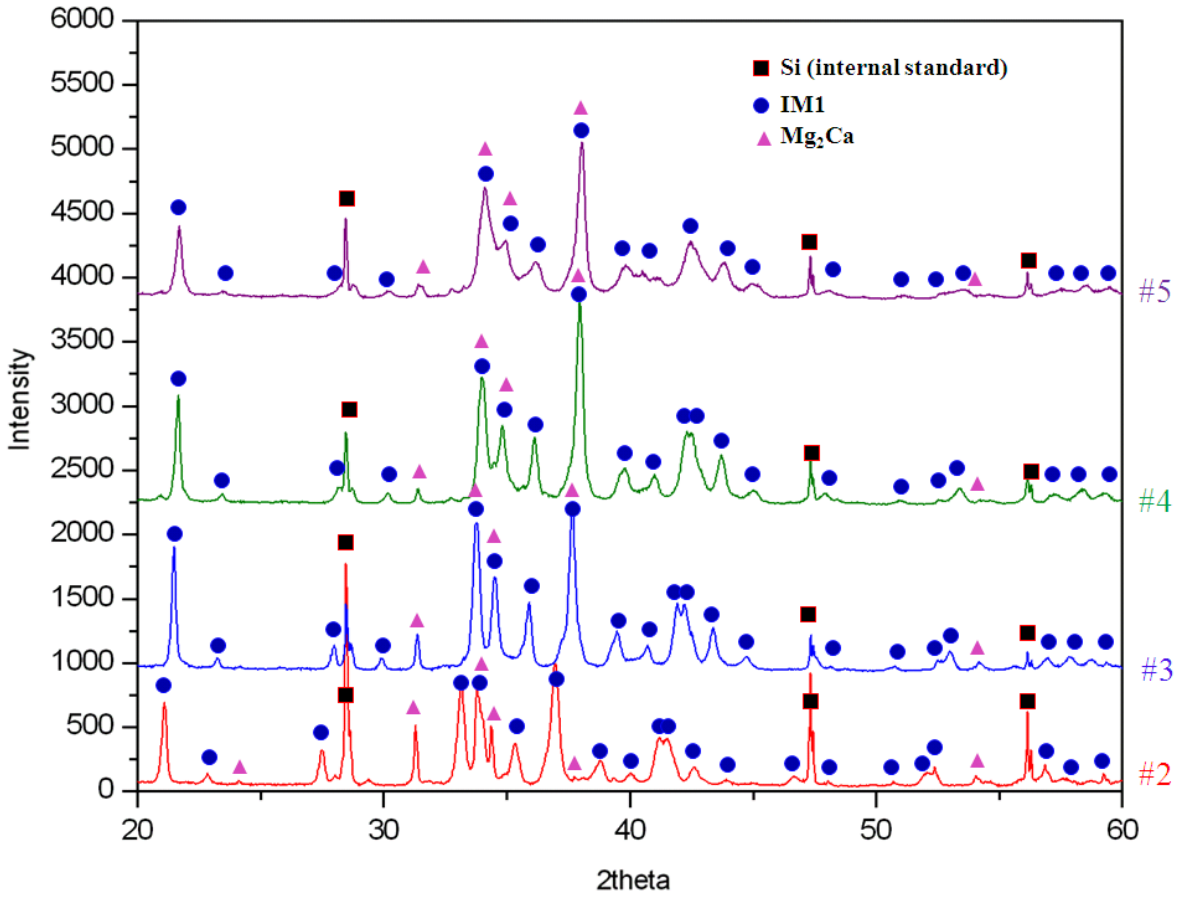

Fig 4.18: XRD patterns of the ternary compound IM1 showing the solid solubility effect.

4.3.1.2 Study of solubility limits of IM1 compound via EPMA and XRD

In order to determine the phase boundaries of IM1 ternary compound, two ternary samples 1 and 6 have been prepared to identify the maximum and minimum solid solubility. Backscattered electron images of these samples are presented in Fig 4.19. Sample 1 contains three phases: IM1, (Mg) and Mg_2Ca. The maximum solid solubility of IM1 has been determined by EPMA as 66.9 at.% Mg. The XRD pattern is illustrated in Fig 4.20(a). This figure demonstrates Rietveld analysis for the IM1, Mg_2Ca and Mg phases in sample 1. Sample 6 contains three phases, the dominating phase is IM1. The minimum solid solubility of IM1 has been determined by EPMA as 25.4 at.% Mg. The

XRD pattern is illustrated in Fig. 4.20(b). $Ca_2Mg_5Zn_{13}$ (IM3) is not detected in the XRD pattern due to its small relative amount. IM2 is a new stoichiometric compound, the prototype has not been reported hence this compound cannot be verified by Rietveld analysis.

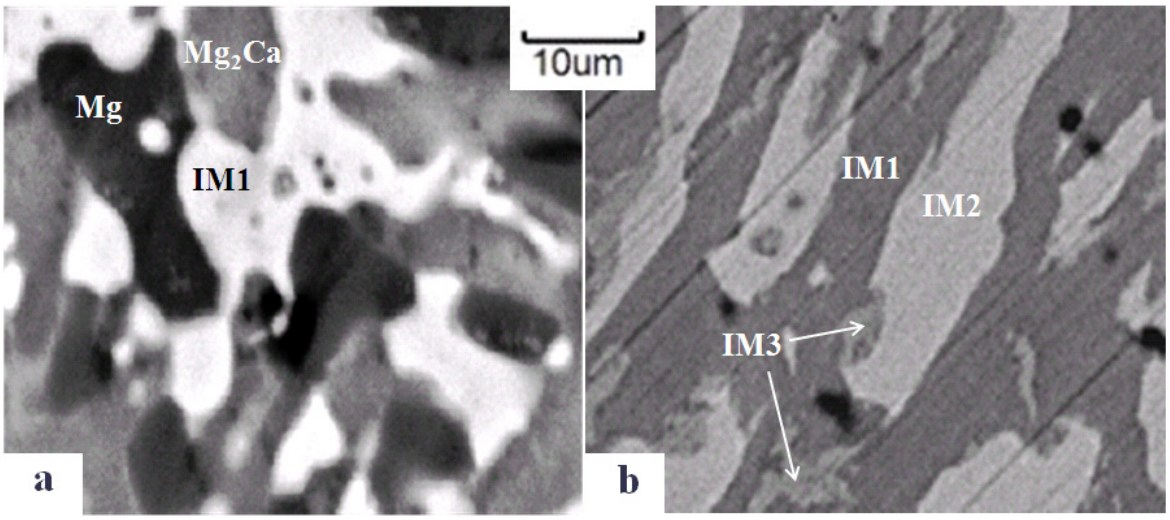

Fig 4.19: BE images: (a) sample 1, (b) sample 6. Both are annealed at 335ºC for 4 weeks.

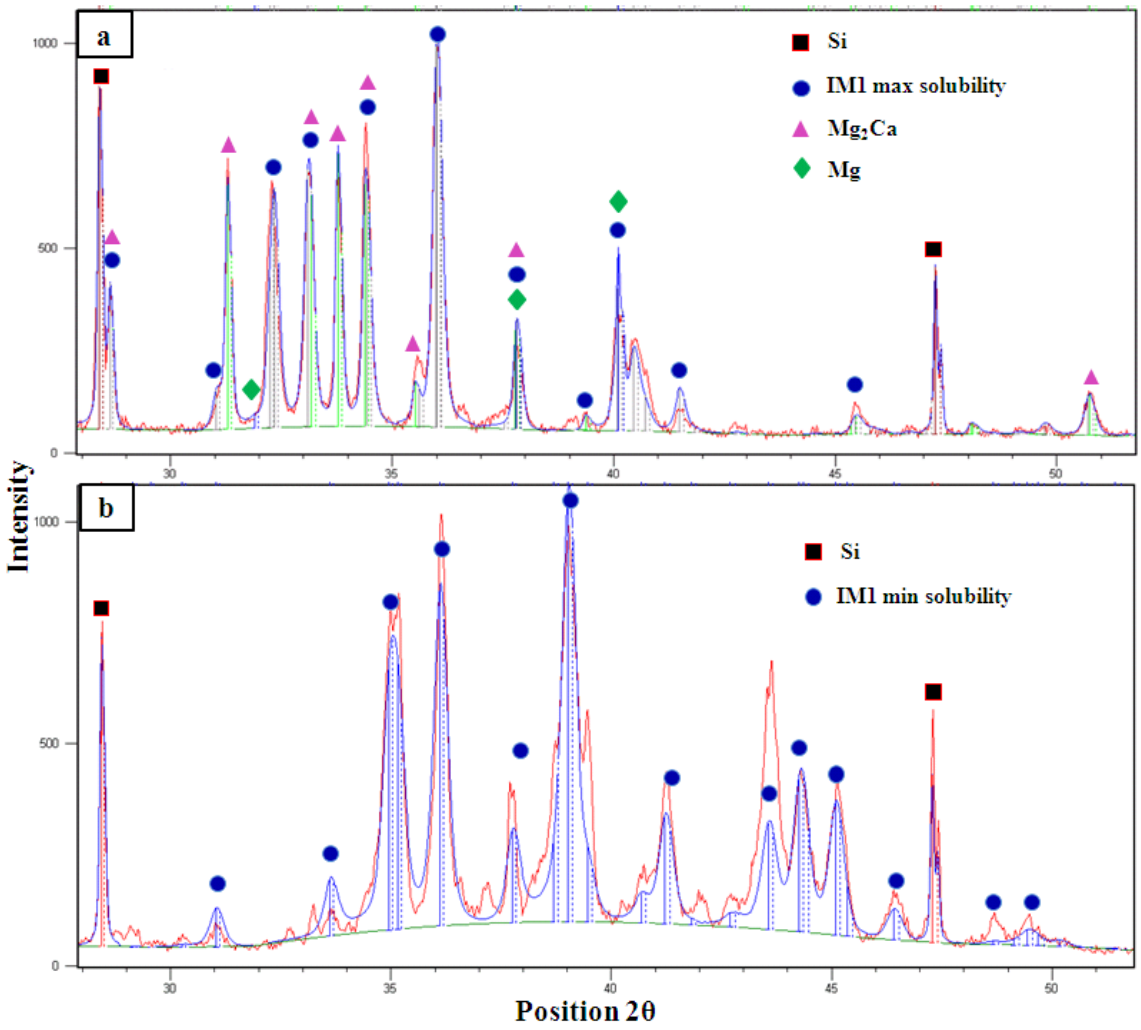

Fig 4.20: Rietveld analysis: (a) sample 1, (b) sample 6. Both are annealed at 335ºC for 4 weeks.

Combining the EPMA results of the solid-solid diffusion couple and key alloys, the actual composition of the Mg-rich ternary compound and its complete homogeneity range have been determined. Taking into account the structure type of IM1, the formula of this compound is $Ca_3Mg_xZn_{15-x}$ ($4.6 \leq x \leq 12$) at 335°C. The actual chemical composition of this ternary compound has been measured quantitatively by EPMA, which shows great consistency with the results obtained by Rietveld approach, as summarized in Table 4.3. Furthermore, refinement of the XRD patterns has been carried out. All XRD data has shown that this solid solution, in six samples, crystallizes in hexagonal structure with

P63/mmc (194) space group and $Sc_3Ni_{11}Si_4$ prototype. Fig 4.21 shows the cell parameters variations with Mg concentration, where substitution of Mg by Zn decreases the unit cell parameters *a* and *c* (Å), and the lattice volume ($Å^3$). This is shown in more details in Table 4.3. The linear relation between the lattice parameters, lattice volume and Mg concentration obeys Vegard's law [36] indicating clearly the occurrence of substitutional solid solubility. The composition $Ca_2Mg_6Zn_3$ reported by Clark [16] and Jardim et al. [19] is very close to sample 2, and they reported consistent unit cell parameters with the current work, as can be observed in Table 4.3 and Fig 4.21.

4.3.1.3 Study of lattice parameters of IM1 compound by Rietveld analysis

The degree of refinement in the Rietveld analysis is judged by the goodness of fit, s, which is calculated as follows:

$$s = (R_{wp}/R_e)^2 \quad \text{..... (4.1)}$$

Where R_{wp} is the weighted summation of residuals of the least squared fit and R_e is the value statistically expected. Therefore an *s* value of 1.0 indicates perfect fit. In order to achieve an acceptable goodness of fit, Rietveld analysis has been carried out to study the fractional atomic coordinates and occupancy. Table 4.4 shows the refined structural parameters of the IM1 compound and the reliability factors. The decrease in all unit cell parameters is in favor of the occupation of 6h sites by Zn from sample 1 to sample 2. The prerequisite substitutional position of 6h sites has also been confirmed by the shortest bond lengths of Mg1-x (x=Ca, Zn, Mg1, Mg2, Mg3) in sample 1, as can be seen in Table 4.5. Most of the bond lengths with Mg1 (6h atomic sites) demonstrate relatively short distance, indicating that the Mg1 position has higher potential to be substituted by Zn

because of the smaller size of Zn atom. For instance, the bond length of Mg2-Mg1 is 3.1014Å, and the distance between Mg2-Mg2, Mg2-Mg3 and Mg2-Mg4 is 3.4156Å, 3.1234Å and 3.2660Å, respectively. It is obvious that the bond length of Mg2-Mg1 shows the shortest distance, suggesting that the Mg1 atomic position is in favor of the substitution of magnesium by Zinc. Once the 6h sites are occupied completely by Zn atoms, as in the fictitious $Ca_2Mg_6Zn_4$ compound, Mg atoms start to be replaced in 4f, 2b and 12k sites by Zn simultaneously. The fractional atomic occupancy of 6h, 4f, 2b and 12k sites of IM1 have been determined as a function of the Mg concentration, as shown in Fig 4.22. Crystallographic and the site occupancy data of $MgYZn_3$ [37] are similar to those for IM1 solid solution. The occupancy of 6h, 4f and 12k sites show good consistency with the current experimental results obtained by Rietveld analysis. The occupancy of 2b sites has not been used in this comparison, because it involves mixing of both Y and Mg atoms, whereas in the current case, this site is occupied by Mg and Zn atoms (Y atom is analogous to Ca not to Zn atom).

The coordination spheres and atomic substitution of Mg by Zn for the different atomic sites have been identified, as can be seen in Fig 4.23. The atomic environment types of 6h, 4f and 12k form icosahedrons, whereas 2b sites have a tricapped trigonal prism atomic environment type with the additional three Ca atoms on the sides of the prisms.

Table 4.3: The chemical composition and unit cell parameters of the IM1 compound determined by EPMA and Rietveld analysis.

Sample No.	Composition of IM1 compound identified by EPMA			IM1 phase composition identified by Rietveld analysis			hexagonal crystal structure, space group $P6_3/mmc$(194) and prototype $Sc_3Ni_{11}Si_4$		
	Ca	Mg	Zn	Ca	Mg	Zn	Unit cell parameters and lattice volume		
							a(Å)	c(Å)	V(Å3)
1	16.7	66.9	16.4	16.7	66.6	16.7	9.958	10.395	892.710
2	16.7	56.1	27.2	16.7	54.5	28.4	9.734	10.169	834.319
3	16.7	47.8	35.5	16.7	46.2	37.1	9.558	10.013	792.139
4	16.7	43.3	40.0	16.7	43.4	39.9	9.486	9.950	775.369
5	16.7	42.1	41.2	16.7	41.9	41.4	9.464	9.925	769.913
6	16.7	25.4	57.9	16.7	25.4	57.9	9.225	9.522	701.803
Paris [14] (metallography)	16.7	41.6	41.6	-			-		
Clark [16] (XRD)	-			18.2	54.5	27.3*	9.725	10.148	831.17
Jardim [19] (TEM/EDS)	18.2	54.5	27.3*	-			9.7	10	814.84

*Recalculated from the $Ca_2Mg_6Zn_3$ formula.

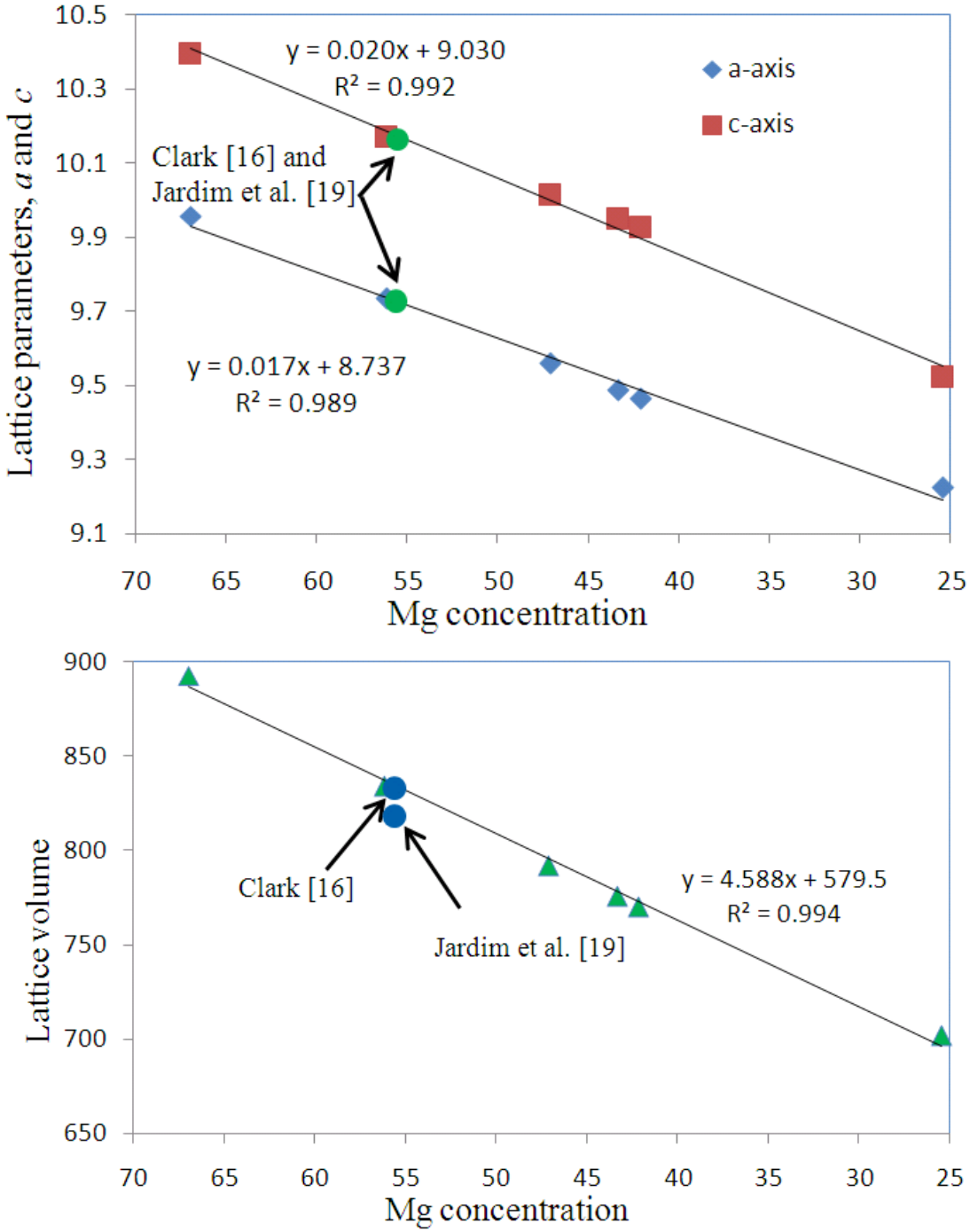

Fig 4.21: Cell parameters with Mg concentration for the IM1 compound, where progressive substitution of Mg by Zn decreases the unit cell parameters *a* and *c* and the lattice volume.

Table 4.4: Refined crystal structure parameters of the IM1 solution compound.

Samples No.	Atomic coordinates (Wyckoff Position)	*Occupancy (%)*	Reliability factors*		
			R_e	R_{wp}	s
1	Ca - 6h Zn1 - 6g Mg1 - 6h Mg2 - 12k Mg3 - 4f Mg4 - 2b	*Ca 100.0* *Zn 99.9* *Mg 100.0* *Mg 100.0* *Mg 100.0* *Mg 100.0*	12.1	15.8	1.71
2	Ca - 6h Zn1 - 6g Mg,Zn1 - 6h Mg2 - 12k Mg3 - 4f Mg4 - 2b	*Ca 100.0* *Zn 99.8* *Mg 26.9* *Mg 100.0* *Mg 100.0* *Mg 100.0*	11.2	16.9	2.27
3	Ca - 6h Zn1 - 6g Zn2 - 6h Mg,Zn2 - 12k Mg,Zn3 - 4f Mg,Zn4 - 2b	*Ca 99.9* *Zn 100.0* *Zn 100.0* *Mg 97.7* *Mg 80.8* *Mg 82.2*	11.0	20.5	3.44
4	Ca - 6h Zn1- 6g Zn2 - 6h Mg,Zn2 - 12k Mg,Zn3 - 4f Mg,Zn4 - 2b	*Ca 100.0* *Zn 100.0* *Zn 99.8* *Mg 94.8* *Mg 71.1* *Mg 82.2*	10.4	20.5	3.87
5	Ca - 6h Zn1 - 6g Zn2 - 6h Mg,Zn2 - 12k Mg,Zn3 - 4f Mg,Zn4 - 2b	*Ca 100.0* *Zn 100.0* *Zn 100.0* *Mg 93.3* *Mg 66.2* *Mg 64.5*	10.3	19.6	3.61
6	Ca - 6h Zn1 - 6g Zn2 - 6h Mg,Zn2 - 12k Mg,Zn3 - 4f Mg,Zn4 - 2b	*Ca 100.0* *Zn 99.8* *Zn 100.0* *Mg 59.5* *Mg 31.3* *Mg 40.7*	10.9	22.3	4.18

* Reliability factors: s presents the goodness of fit; R_{wp} is the weighted summation of residuals of the least squared fit; R_e is the value statistically expected.

Table 4.5: Atomic bond lengths of the IM1 compound in sample 1.

Atom1	Atom2	Distance (Å)
Mg2	Ca	3.5291
Mg2	Ca	3.5234
Mg2	Mg2	3.3052
Mg2	Mg2	3.4156
Mg2	Mg1	***3.1014***
Mg2	Mg3	3.1234
Mg2	Mg4	3.2660
Ca	Mg3	3.4984
Ca	Mg4	3.3117
Ca	Ca	4.2224
Ca	Mg1	3.4446
Ca	Zn1	3.7352
Mg2	Zn1	3.0540
Mg1	Zn1	***2.8088***
Mg3	Zn1	2.8761
Mg1	Mg1	3.1329
Mg1	Mg3	3.2399

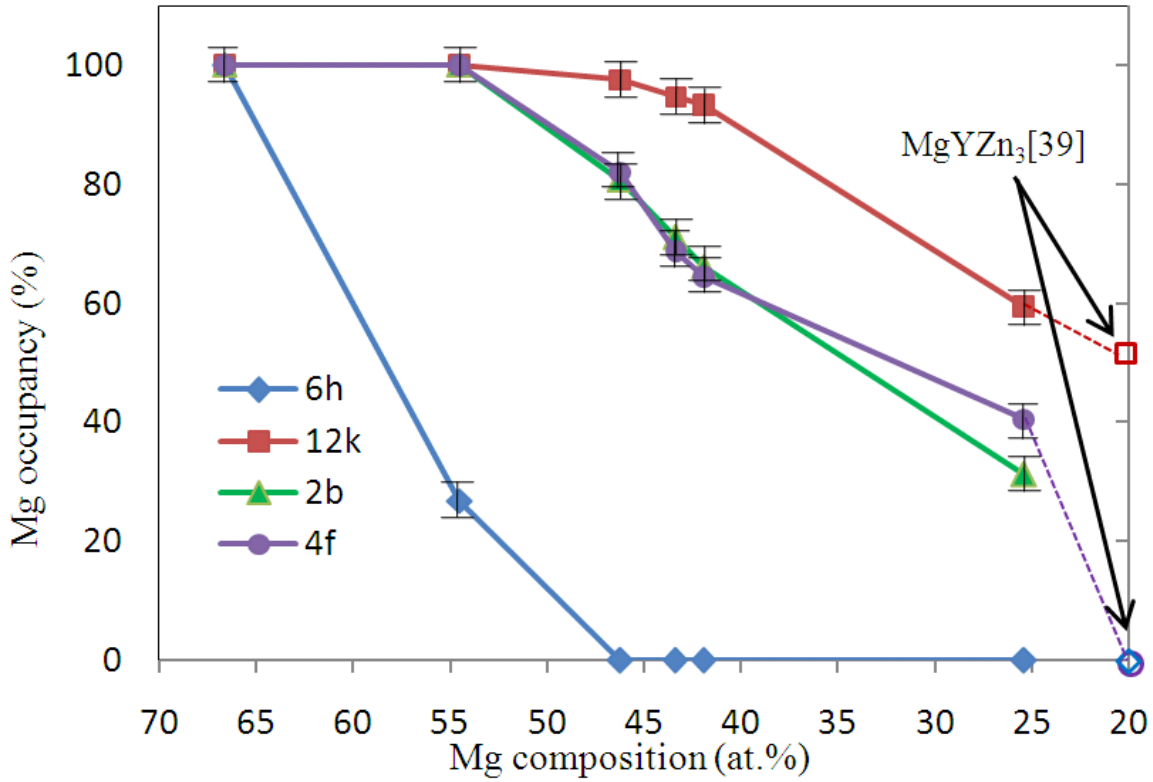

Fig 4.22: Mg occupancy in the IM1 compound as a function of Mg concentration.

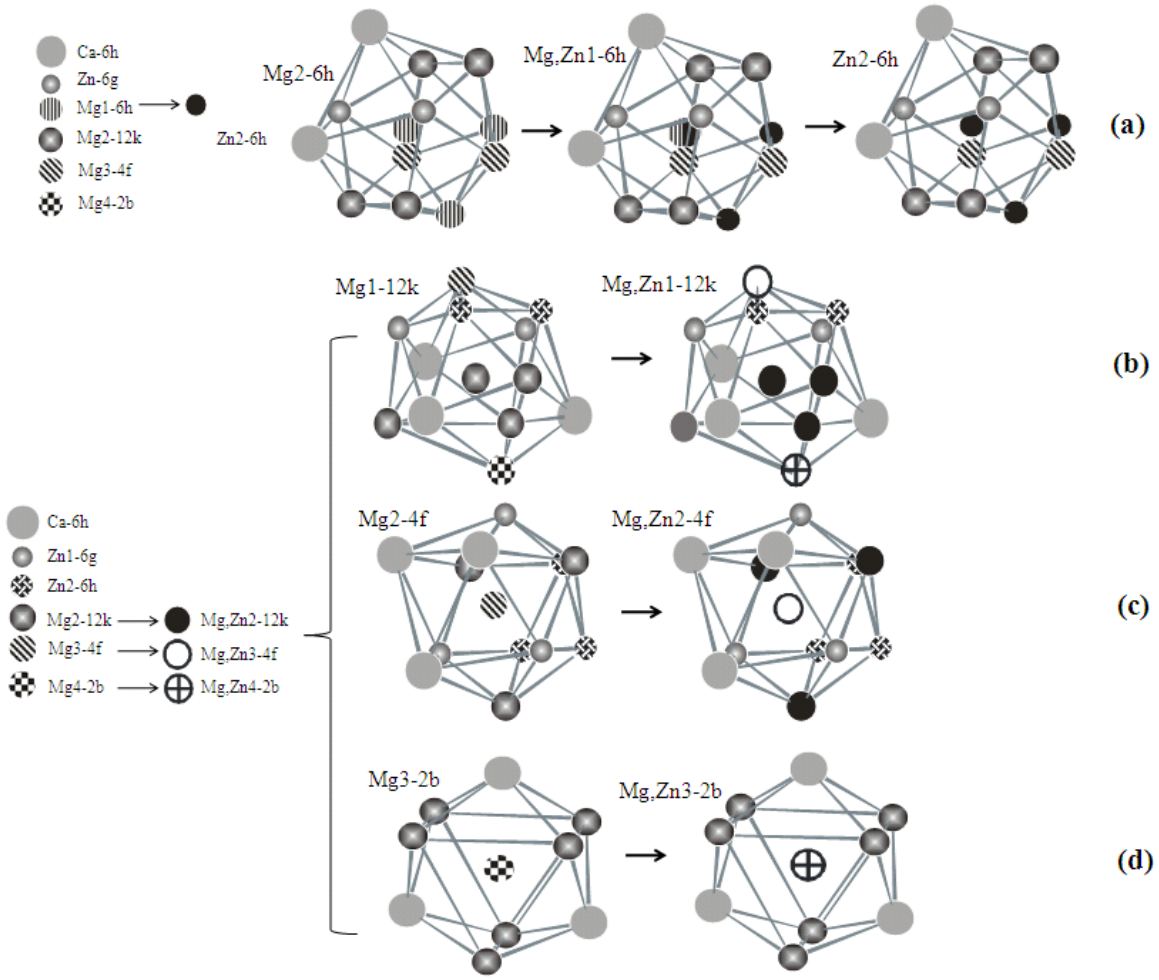

Fig 4.23: The coordination spheres of dynamic atomic substitution of magnesium by zinc with different atomic coordinates: (a) substitution of Mg atoms by Zn atoms on 6h sites until they are completely occupied by Zn atoms; (b) to (d) the simultaneous substitution of Mg atoms by Zn atoms on the 12k, 4f and 2b atomic sites.

4.3.1.4 Study of crystal structure of IM1 compound via TEM

The structure of IM1 single phase region has been studied by TEM. Focused Ion Beam (FIB) is used to lift a specimen of the ternary compound from sample 4 ($Ca_{18.0}Mg_{44.2}Zn_{37.8}$), as shown in Fig 4.24(a). According to the crystallographic data obtained by XRD, the hexagonal structure has been indexed and confirmed by means of Selected Area Electron Diffraction (SAED) data, as shown in Fig 4.24 (b) and (c). The planar spaceing, *d* values, obtained from the SAED pattern of sample 4 shows good

consistency with the XRD results, as can be seen in Table 4.6. Furthermore, because of the difference in solid solubility between samples 4 and 2, *d* values determined from sample 2 are slightly larger than those from sample 4 corresponding to the higher content of the larger Mg atom in sample 2. Even though Jardim et al. [19] reported different structure type, the *d* values calculated from the SAED pattern can be used to compare with the values obtained by XRD from sample 2, since sample 2 and $Ca_2Mg_6Zn_3$ have the sample IM1 compound composition. The SAED pattern reported by Jardim et al. [19] as shown in Fig 4.24(d). It is clearly shown that both series of *d* values obtained from XRD pattern reported by Clark [16] and SAED pattern reported by Jardim et al. [19] show good consistency with the values determined by XRD from sample 2, as detailed in Table 4.6. In addition, the consistent results of *d* and (hkl) values obtained from XRD and SAED patterns support the fact that this ternary compound has the said hexagonal structure.

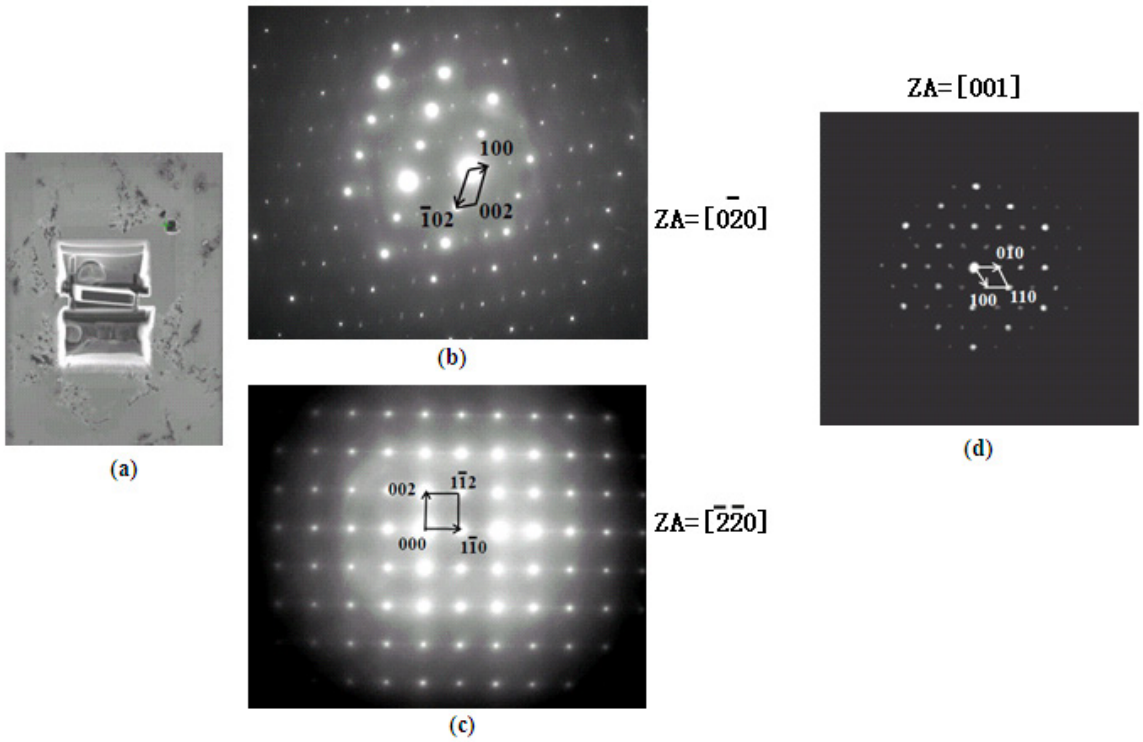

Fig 4.24: (a) Using FIB to lift a specimen of the ternary compound; (b) SAED pattern of the sample 4 [0$\bar{2}$0] zone axis indexed as a hexagonal structure; (c) SAED pattern of the sample 4 [$\bar{2}\bar{2}$0] zone axis indexed as a hexagonal structure; (d) SAED pattern of $Ca_2Mg_6Zn_3$ [001] zone axis reported by Jardim et al. [19].

Table 4.6: Comparison of planar space (*d* value (hkl)) of the IM1 compound in samples 2 and 4.

(hkl)	*d* (Å) (sample 4)		*d* (Å) (sample 2)		
	By XRD (in this work)	From SAEDP (in this work)	By XRD (in this work)	From JCPDS card (Clark [16])	From SAEDP (Jardim et al. [19])
100	8.211	8.223	8.440	8.400	8.4
002	4.975	4.958	5.064	5.100	5.0
110	4.743	4.760	4.867	4.900	4.85
102	4.251	4.275	4.351	-	4.36
112	3.430	3.460	3.514	-	-
300	2.731	2.724	2.809	2.800	-
004	2.486	2.479	2.527	2.530	-
220	2.370	2.380	2.433	2.430	-
114	2.202	2.223	2.253	2.250	-
222	2.140	2.148	2.194	2.190	-
224	1.723	1.728	1.757	1.752	-

4.3.1.1 Study of sublattice model of IM1 compound

Moreover, modeling of an intermetallic solid solution requires information regarding the crystal structure of the phases and their homogeneity ranges. From the crystallographic data obtained in this work, the following sublattice model is applied to represent the current compound:

$(Ca)_6(Zn)_6(Mg,Zn)_6(Mg,Zn)_{12}(Mg,Zn)_4(Mg,Zn)_2$ – *Model I*

Considering the atomic positions and site occupancy from the current experimental results, the atomic occupancy of 4f and 2b demonstrate the same tendency, as shown in Fig 4.22. Thus, these two sites should be coupled to reduce the number of end members. The sublattice model can be modified to:

$(Ca)_6(Zn)_6(Mg,Zn)_6(Mg,Zn)_{12}(Mg,Zn)_6$ – *Model II*

Model II can be simplified further in order to have a more practical sublattice model suitable for thermodynamic modeling of this compound. This can be achieved using the similarity in the coordination numbers and the site occupancy information obtained in this work. The final model for this compound can be written as:

$(Ca)(Zn)(Mg,Zn)_4$ – *Model III*

This model provides a solubility range of $0 \leq Mg \leq 66.7$ at.% and $16.7 \leq Zn \leq 83.3$ at.%, which covers the wide homogeneity range of the $Ca_3Mg_xZn_{15-x}$ ($4.6 \leqslant x \leqslant 12$ at 335°C) compound.

4.3.2 Phase boundaries of the Mg_2Ca compound and phase relations among Mg_2Ca, IM1 and Mg solid solutions

In order to study the phase boundaries of the Mg_2Ca compound and the phase relations among Mg_2Ca, IM1 and Mg solid solutions, seven ternary key samples (1 to 5, 7, 8) have been prepared, as illustrated in Fig 4.16. The compositions and phase identification of these samples are summarized in Table 4.7. The actual chemical compositions of the alloys are measured by ICP and the composition of Mg_2Ca compound has been measured quantitatively by EPMA/WDS. The phase relations obtained from EPMA are consistent with those from XRD. Backscattered electron image of sample 7 annealed at 335ºC for 4 weeks is presented in Fig 4.25(a). The equilibrium microstructure consists of three phases: (Mg_2Ca), CaZn and $CaZn_2$. The Mg_2Ca form substitutional solid solution where Zn substitutes Mg atoms while Ca content remains constant at 33.3 at.%, the solid solubility limit has been identified by EPMA as 10.8 at.% Zn. In order to verify the EPMA findings, this sample has been studied by XRD using Rietveld analysis. The XRD pattern is illustrated in Fig 4.25(b). Full pattern refinement has been carried out. However, the EPMA and XRD results obtained from samples 1 to 5 clearly show that the Mg_2Ca phase has complex solid solution, where Zn atoms substitute both Ca and Mg atoms. Fig 4.26 and Table 4.8 show the cell parameters variations with Zn concentration from sample 1 to 5, where substitution of Ca and Mg by Zn decreases the unit cell parameters *a* and *c*, and the lattice volume. Table 4.8 shows the refined structural parameters of the Mg_2Ca compound and the reliability factors. The least squares approximation is used to establish the relation between the lattice parameters and Zn concentration. The cell parameters *a* and *c* extrapolated at 10.8 at.% Zn concentration (the solubility limit determined by

EPMA where Mg is only substituted by Zn atom not Ca) are used to compare with the results obtained from samples 7 and 8, as can be seen in Fig 4.26. This figure clearly shows that the unit cell parameters of samples 1 to 5 are smaller than those of samples 7 and 8. Such behavior is understandable considering the atomic sizes of elements. According to the Periodic Table [38], the metallic radii of Ca, Mg and Zn are 180, 150 and 130pm, respectively. Hence, the unit cell parameters, where Zn substitutes both Mg and Ca atoms, should be smaller than those, where Zn just substitutes Mg atoms. The experimental results on solid solubility of the Mg_2Ca compound at 335ºC have been confirmed by both EPMA and XRD techniques proving the existence of complex solid solution. The homogeneity ranges and phase relations among the Mg_2Ca, Mg and IM1 phases have been collected and analyzed, as demonstrated in Fig 4.27.

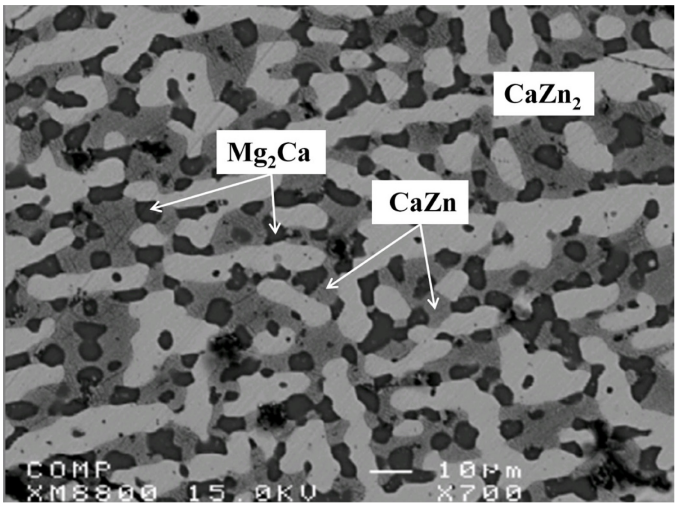

(a)

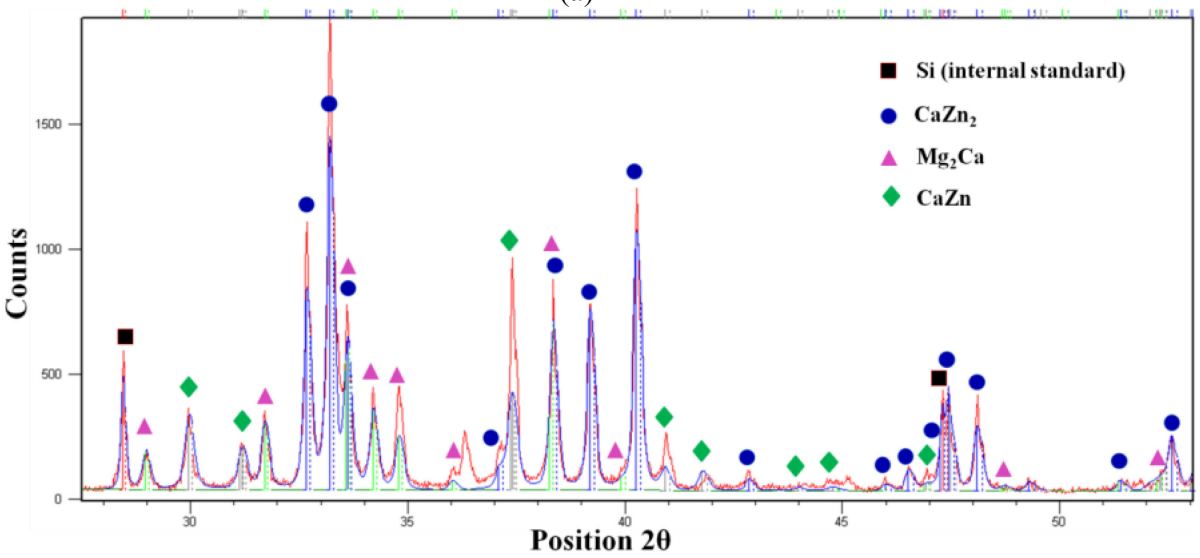

(b)

Fig 4.25: Sample 4 annealed at 335ºC for 4 weeks: (a) SEM BSE image; (b) Rietveld analysis.

Table 4.7: The actual composition of the key samples and the phases present.

Sample No.	Actual composition identified by ICP (at.%)			Phases identification		Composition of Mg_2Ca identified by EPMA		
	Ca	Mg	Zn	By EPMA	By XRD	Ca	Mg	Zn
1	18.8	74.1	7.1	Mg	Mg	32.1	65.0	2.9
				Mg_2Ca	Mg_2Ca			
				IM1	IM1			
2	22.4	59.3	18.3	Mg_2Ca	Mg_2Ca	31.6	64.6	3.8
				IM1	IM1			
3	18.4	48.8	32.8	Mg_2Ca	Mg_2Ca	31.3	64.5	4.2
				IM1	IM1			
4	18.0	44.2	37.8	Mg_2Ca	Mg_2Ca	31.2	64.4	4.4
				IM1	IM1			
5	18.0	42.9	40.3	Mg_2Ca	Mg_2Ca	31.0	64.2	4.8
				IM1	IM1			
6	35.2	36.3	28.5	Mg_2Ca	Mg_2Ca	33.3	55.9	10.8
				$CaZn_2$	$CaZn_2$			
				CaZn	CaZn			
7	40.8	9.8	49.4	Mg_2Ca	Mg_2Ca	33.3	55.9	10.8
				$CaZn_2$	$CaZn_2$			
				CaZn	CaZn			

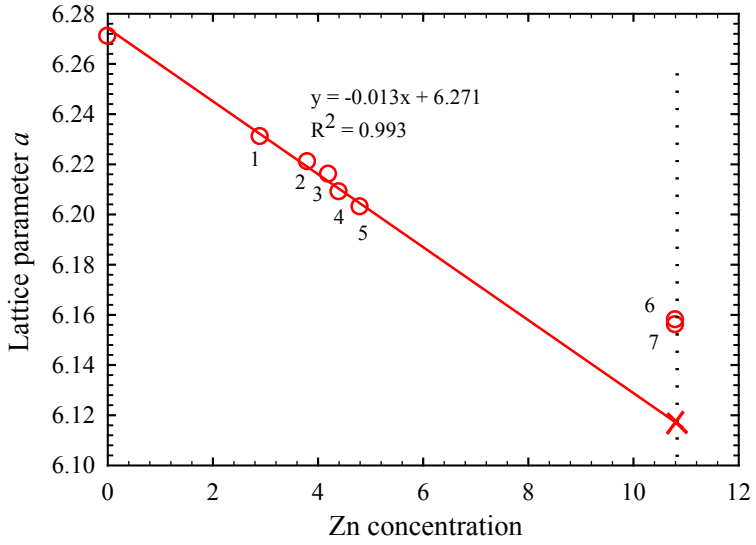

(a)

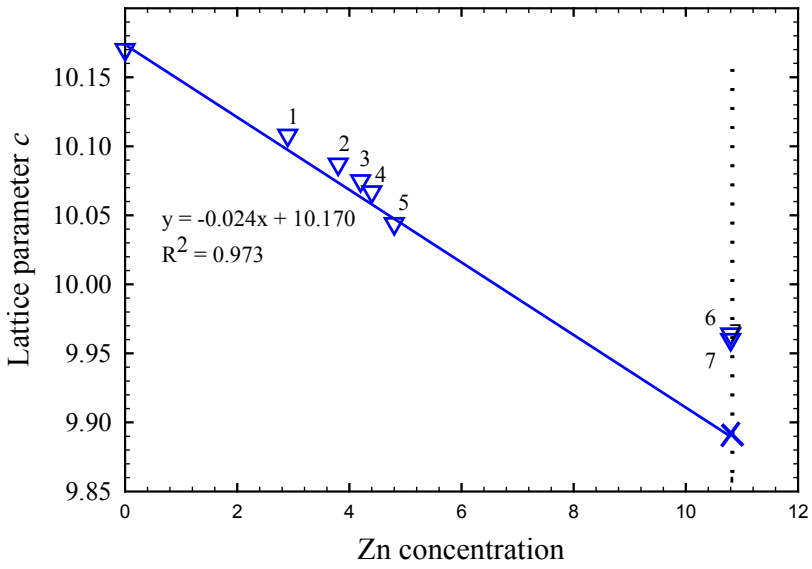

(b)

Fig 4.26: Cell parameters (a) *a* and (b) *c* with Zn concentration in the Mg_2Ca compound, where substitution of Ca and Mg by Zn decreases both cell parameters.

Table 4.8: The chemical composition and unit cell parameters of the Mg_2Ca compound determined by EPMA and Rietveld analysis.

Sample No.	Composition of Mg_2Ca compound identified by EPMA			hexagonal crystal structure, space group $P6_3/mmc$(194) and prototype $MgZn_2$			Reliability factors*		
	Ca	Mg	Zn	Unit cell parameters and lattice volume			R_e	R_{wp}	s
				a(Å)	c(Å)	V(Å3)			
1	32.1	65.0	2.9	6.231	10.108	339.835	12.1	15.8	1.71
2	31.6	64.6	3.8	6.221	10.087	338.002	11.2	16.9	2.27
3	31.3	64.5	4.2	6.216	10.075	337.082	11.0	20.5	3.44
4	31.2	64.4	4.4	6.209	10.067	336.117	10.4	20.5	3.87
5	31.0	64.2	4.8	6.203	10.044	334.796	10.3	19.6	3.61
6	33.3	55.9	10.8	6.156	9.960	326.866	14.1	21.7	2.37
7	33.3	55.9	10.8	6.158	9.964	327.237	11.6	25.2	4.72

* Reliability factors: s presents the goodness of fit; R_{wp} is the weighted summation of residuals of the least squared fit; R_e is the value statistically expected.

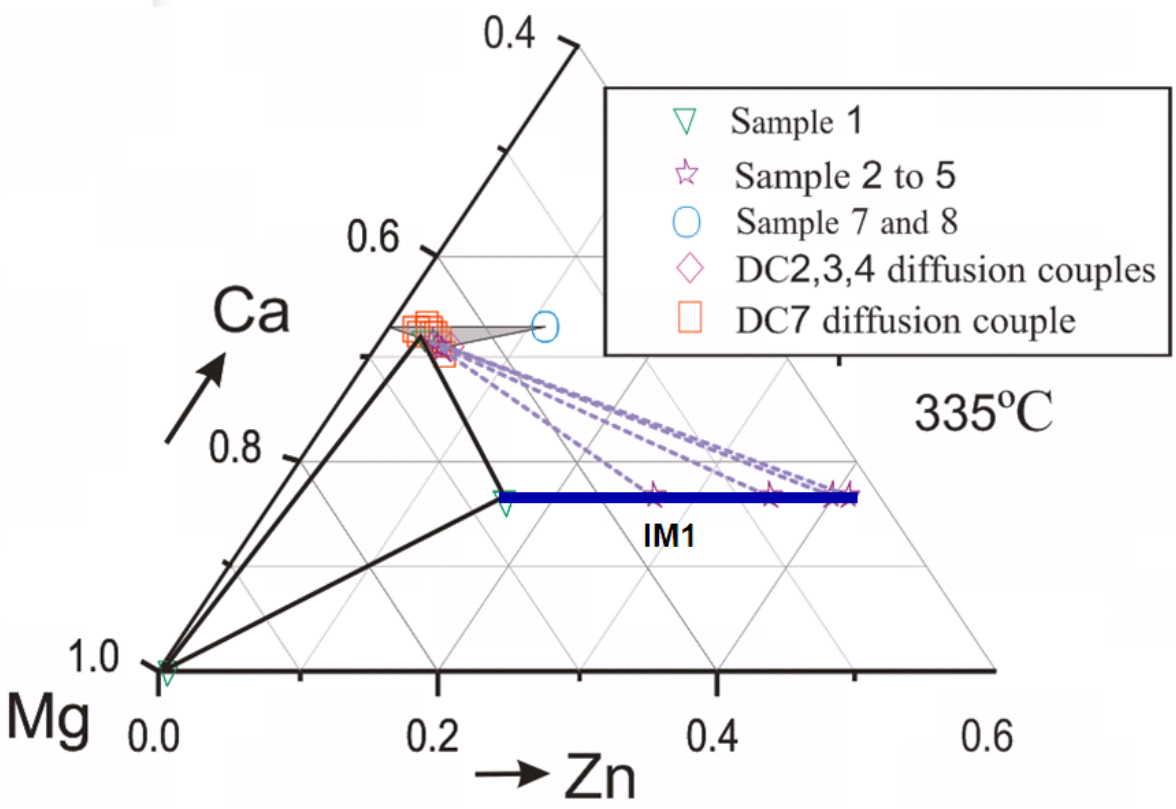

Fig 4.27: Phase boundaries of Mg_2Ca compound and the phase relations among Mg_2Ca, IM1and Mg solid solutions.

4.3.3 Phase relations between IM3 and Mg solid solutions

In order to determine the crystal structure of IM3 compound and phase relations between IM3 and Mg solid solutions, key sample 9 has been prepared, as illustrated in Fig 4.16 and Fig 4.28(a). Backscattered electron image of this sample after annealing at 335ºC is presented in Fig 4.28(a). Quantitative measurement of the elemental concentrations of IM3 and Mg solid solutions has been carried out by means of EPMA. The phase relations obtained from XRD are consistent with the results determined by EPMA. For Mg solid solution, the hexagonal structure has been indexed and confirmed by means of Selected Area Electron Diffraction (SAED) data, as illustrated in Fig 4.28(b). The planar spacing,

d values, obtained from the SAED pattern of sample 9 show good consistency with the XRD results, as can be seen in Table 4.9. Furthermore, *d* values of Mg solid solution determined from sample 9 are slightly smaller than those reported by Latroche et al. [39] due to the higher content of the smaller Zn atom in sample 9. From Table 4.10, it can be seen that substitution of Mg by Zn decreases the lattice parameter *a* and *c* from 3.223 Å and 5.219 Å, for pure Mg [39], to 3.198 Å and 5.188 Å, for the Mg solid solution. According to the crystallographic data of (IM3) compound obtained by XRD, the hexagonal structure has been indexed and confirmed by means of SAED data, as shown in Fig 4.28(c) and (d). The planar spacing, *d* values, obtained from the SAED pattern of sample 9 shows good consistency with the XRD results, as can be seen in Table 4.11.

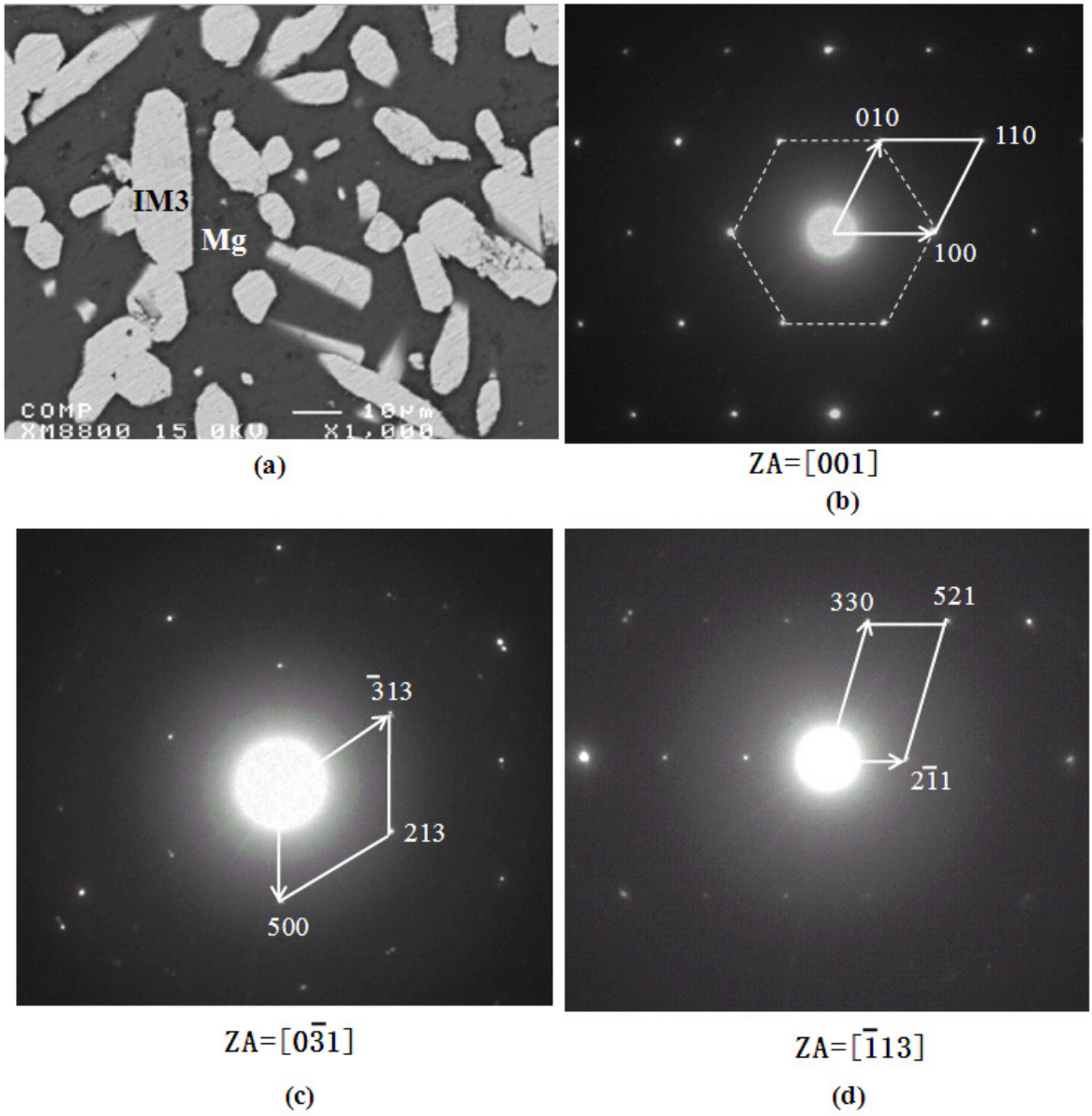

Fig 4.28: (a) SEM BSE image of sample 9; (b) SAED pattern of hexagonal Mg solid solution; (c) SAED pattern of (IM3) [$0\bar{3}1$] zone axis indexed as a hexagonal structure; (d) SAED pattern of (IM3) [113] zone axis indexed as a hexagonal structure.

Table 4.9: Comparison of planar space (*d* value (hkl)) of the Mg solid solution in sample 9.

(hkl)	*d* (Å) (Mg)		
	From SAEDP (in this work)	By XRD (in this work)	[39]
010	2.76	2.769	2.791
002	1.60	1.599	1.611

Table 4.10: Comparison of lattice parameters of the Mg solid solution in sample 9.

Lattice parameters of (Mg)	
a (Å)	*c* (Å)
3.223 [39]	5.219 [39]
3.198 (in this work)	5.188 (in this work)

Table 4.11: Comparison of planar space (*d* value (hkl)) of the (IM3) compound in sample 9.

(hkl)	*d* (Å) (sample 4)	
	From SAEDP (in this work)	By XRD (in this work)
101	7.31	7.250
201	5.23	5.172
300	4.31	4.260
211	4.30	4.235
500	2.56	2.556
213	2.51	2.508
330	2.49	2.460
313	2.27	2.260
511	2.24	2.221
521	1.98	1.993
304	1.97	1.955

4.3.4 Homogeneity range of IM4 and phase relations between (IM3) and IM4

Key samples 10 and 11 have been prepared to determine the homogeneity range of IM4 and the phase relations between IM3 and IM4. Backscattered electron images of these samples annealed at 335ºC are presented in Fig 4.29(a) and (b). The microstructure of sample 10 consists of three phases: (Mg), (IM3) and IM4. Whereas sample 11 consists of: (IM3), $Mg_{12}Zn_{13}$ and IM4. Although the Ca concentration in IM4 is only 1.5 at.%, this is

not an extended solubility of a binary compound because there is no Mg-Zn binary compound around 45 at.% Zn in the Mg-Zn binary system. Hence, IM4 is a new ternary stoichiometric compound with $Ca_{1.5}Mg_{55.3}Zn_{43.2}$ composition. Besides, in a similar system Ce-Mg-Zn, a ternary compound with a similar composition was reported by Kevorkov et al. [40]. The XRD pattern of sample 10 is illustrated in Fig 4.29(c) where the peaks of IM4 ternary phase are not labled. The crystallography determination is still underway by means of TEM.

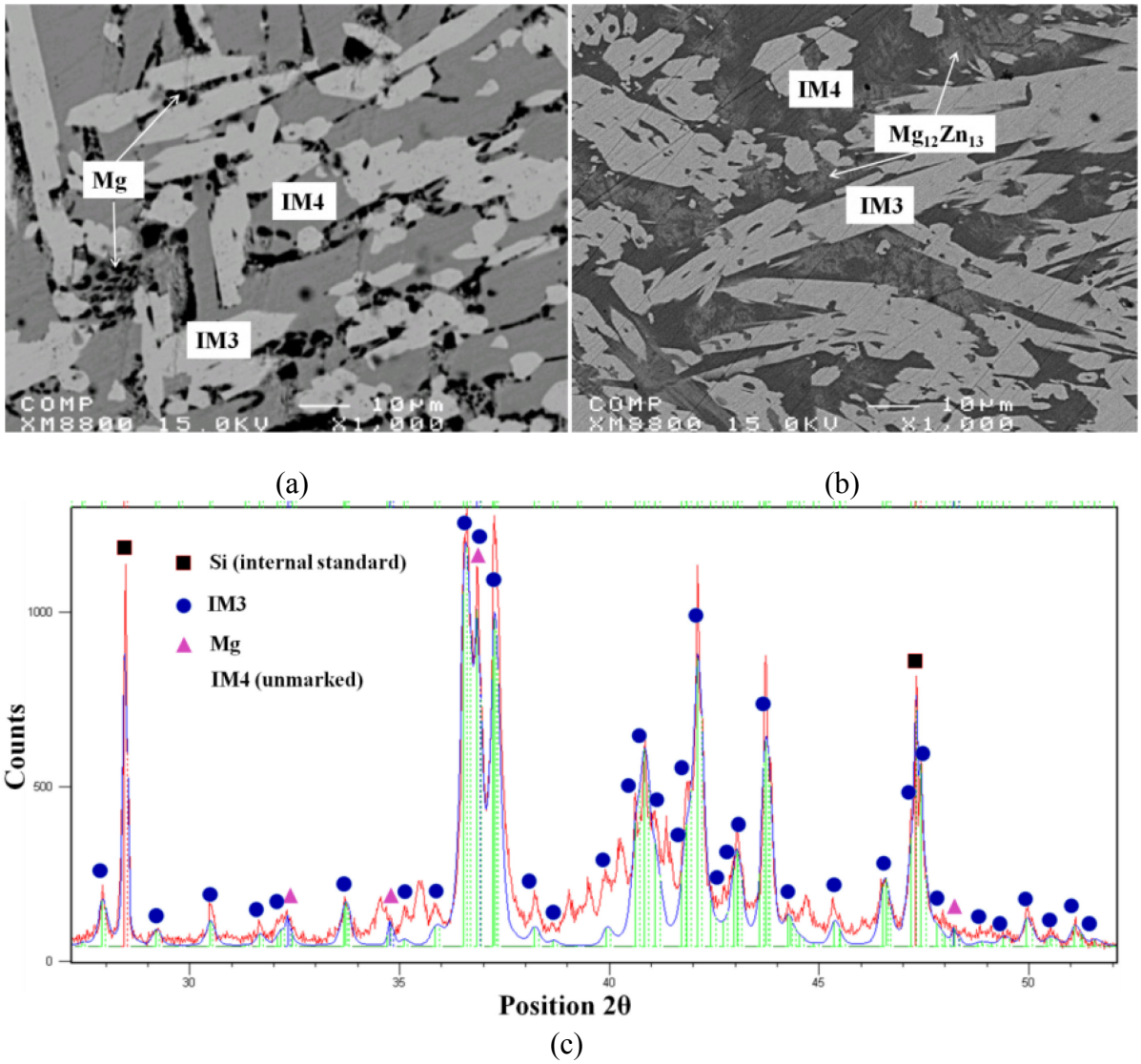

(a) (b)

(c)

Fig 4.29: (a) SEM BSE images of sample 10; (b) SEM BSE images of sample 11; (c) Rietveld analysis of sample 10.

4.3.5 Phase relations in the Zn-rich corner

Key sample 12 has been prepared to study the phase relations in the Zn-rich corner. Backscattered electron image of this sample annealed at 335ºC for 4 weeks is presented in Fig 4.30 (a). The XRD pattern is illustrated in Fig 4.30 (b). Full pattern refinement has been carried out by Rietveld analysis. The results obtained from EPMA and XRD show that this sample has four phases indicating that the equilibrium state has not been reached: (IM3), ($MgZn_2$), ($CaZn_{11}$) and ($CaZn_{13}$). In the Zn-rich corner of the Ca-Zn binary phase diagram, $CaZn_{11}$ is a very stable congruent melting compound with the melting point of 722ºC, and the peritectic transformation of $CaZn_{13}$ occurs at 669ºC. During the process of solidification, $CaZn_{11}$ solid solution precipitates as a primary phase. After heat treatment at 335ºC for 4 weeks, the $CaZn_{11}$ should transform to $CaZn_{13}$ solid solution, but the decomposition process was not complete. Because with relative low heat treatment temperature and stable primary solidification phase, solid-state decomposition process is very sluggish. True equilibrium must be very difficult to reach in this sample. Therefore, in order to avoid those alloys with very sluggish decomposition kinetics, diffusion couple technique has the advantage to form equilibrium phases and has been used in the present work.

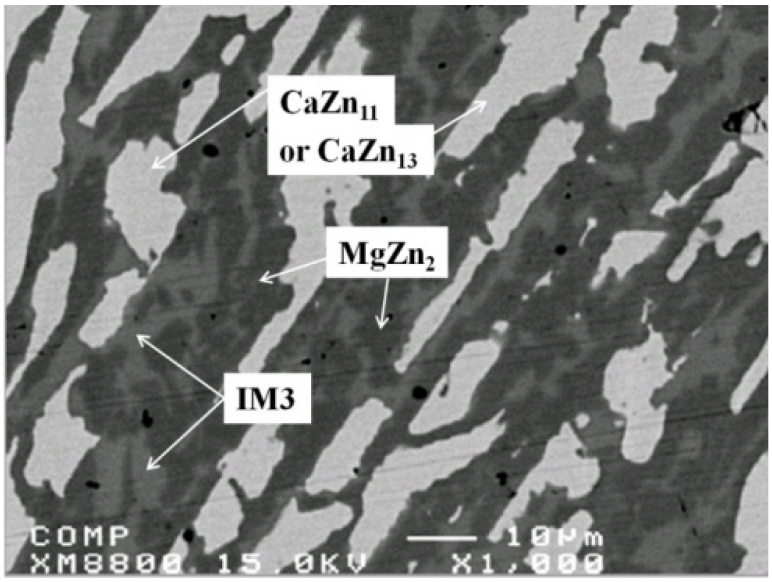

(a)

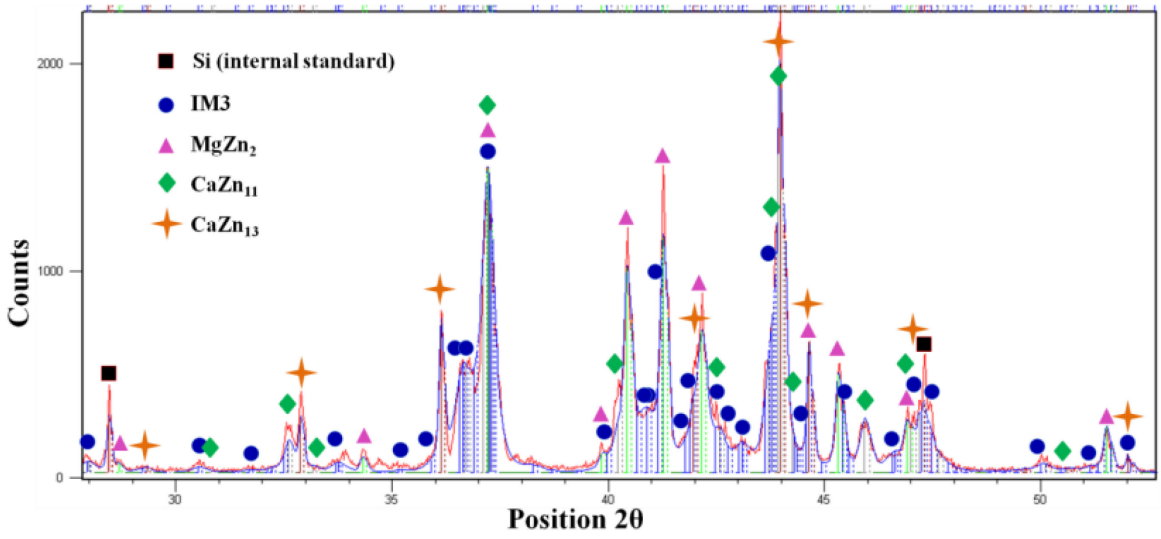

(b)

Fig 4.30: Sample 12 annealed at 335ºC for 4 weeks: (a) SEM BSE image; (b) Rietveld analysis.

4.4 The Ca-Mg-Zn isothermal section at 335 ºC

Combining the results obtained from 9 diffusion couples and 32 key alloys, the isothermal section of the Ca-Mg-Zn phase diagram at 335ºC has been constructed and

presented in Fig 4.31. The 335ºC isothermal section of Ca-Mg-Zn system based on the current experimental work compared with that calculated from Wasiur-Rahman and Medraj [12] is present in Fig. 4.32. The experimental data can be used for CALPHAD modeling and the re-optimization of this system.

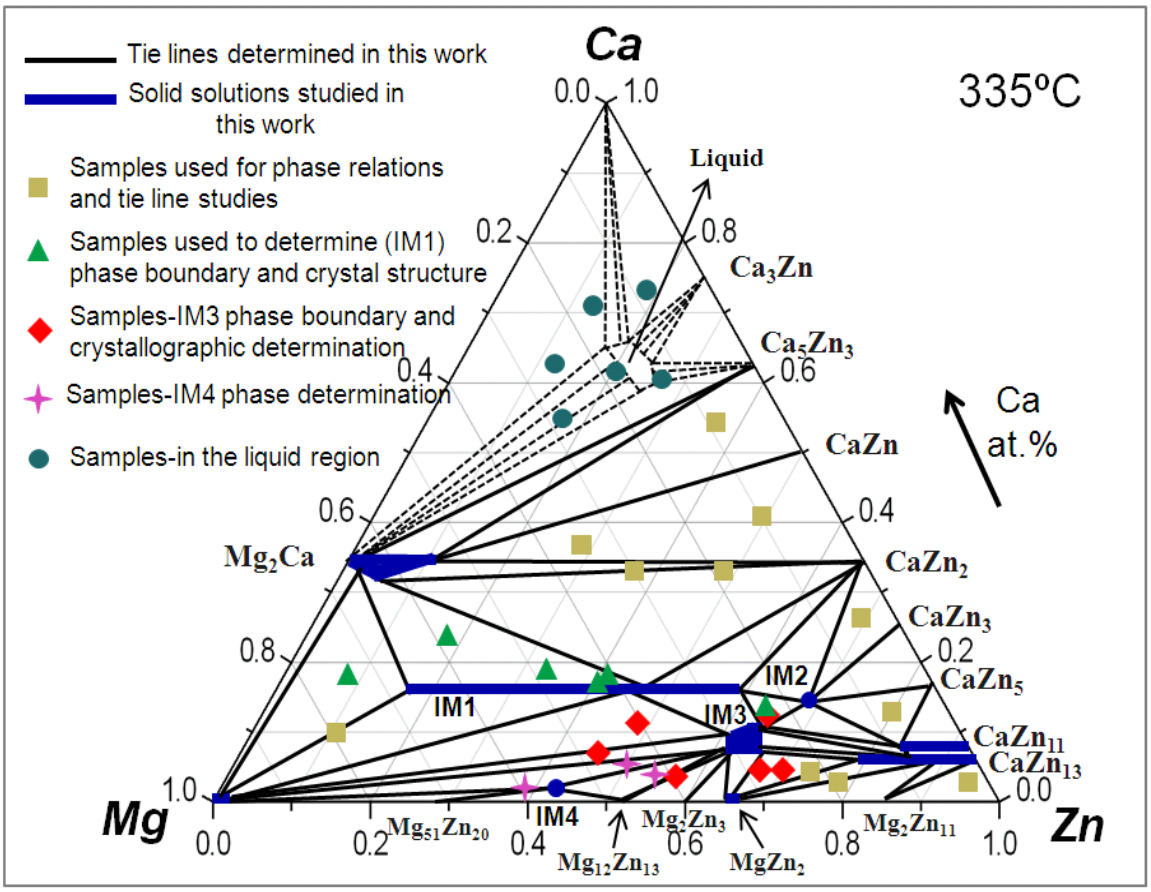

Fig 4.31: The 335ºC isothermal section of Ca-Mg-Zn system constructed from nine diffusion couples and 32 key samples.

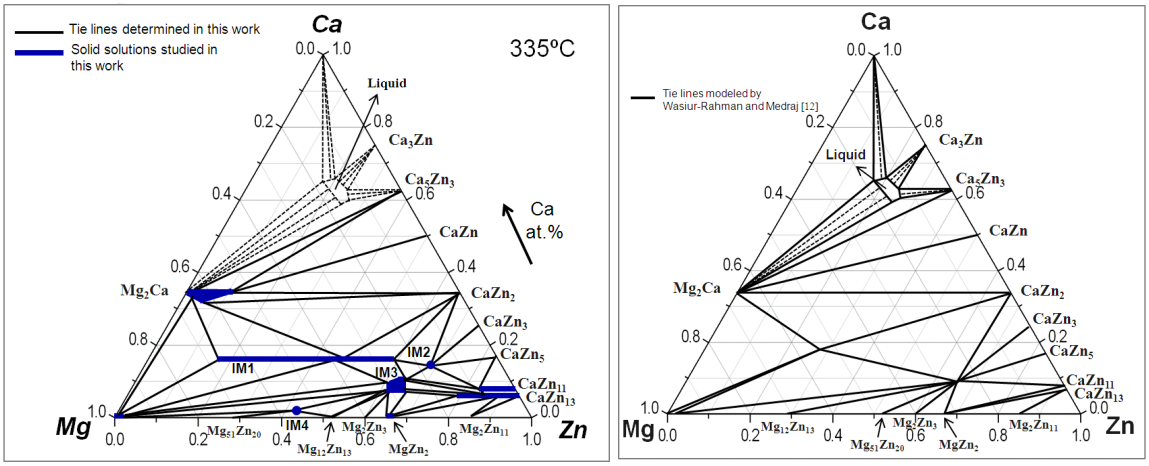

Fig 4.32: The 335ºC isothermal section of Ca-Mg-Zn system based on the current experimental work compared with that calculated from Wasiur-Rahman and Medraj [12].

CHAPTER 5

Concluding Remarks, Contributions and Suggestions for Future Work

4.1 Concluding remarks

A combination of high throughput diffusion couple technique and selected equilibrated key alloys have been used to construct the Ca-Mg-Zn isothermal section at 335ºC. Phase relations, solubility limits and crystallographic information have been determined for binary and ternary compounds using SEM, EPMA, EBSD, TEM and XRD techniques. Four ternary compounds have been found in this system, the composition and homogeneity ranges of IM1 and IM3 have been determined. IM2 and IM4 are new compounds, both of them have been studied for the first time and are considered to be stoichiometric. The formula of IM1 compound is $Ca_3Mg_xZn_{15-x}$ ($4.6 \leq x \leq 12$) at 335°C. It has hexagonal structure with P63/*mmc* (194) space group and $Sc_3Ni_{11}Si_4$ prototype. The lattice parameters of this compound increase linearly with increasing Mg content obeying Vegard's law. The site occupancy of 6h, 4f, 2b and 12k has been presented as a function of Mg concentration. Selected area electron diffraction data, obtained by TEM, and the planar spacing *d* values obtained by Rietveld analysis demonstrate excellent consistency. Combining the atomic occupancy results and the crystallographic details obtained in this work, a three sublattice $(Ca)(Zn)(Mg,Zn)_4$ model is suggested for this compound.

Three binary compounds: $CaZn_{11}$, $CaZn_{13}$ and Mg_2Ca have been found to have an extended solid solubility in the ternary system. A mechanism explaining the evolution of the different morphologies in the diffusion couples has been proposed. Depending on the different terminal compositions of diffusion couples, the morphological evolution can be: 'tooth-like' morphology, matrix phase with either isolated or dendritic shape precipitates morphology, or uniform layer morphology.

5.2 Contributions

A combination of high throughput diffusion couple technique and selected equilibrated key alloys have been used to construct the Ca-Mg-Zn phase diagram in the present work and the following contributions can be seen:

- The solid solubility and crystal structure of IM1, IM3 ternary compounds have been determined and confirmed by means of SEM, EPMA, XRD, EBSD and TEM. The contradictions surrounding their composition and structure have been resolved.
- Two new ternary compounds IM2 and IM4 in the Ca-Mg-Zn system have been discovered in this work.
- The solid solubility of $CaZn_{11}$, $CaZn_{13}$ and Mg_2Ca binary compounds extended in the ternary system has been determined for the first time using diffusion couples and key alloys.
- A mechanism explaining the evolution of the different morphologies in the diffusion couples has been proposed in the present research.

During the course of the current thesis research, the following journal publications and presentations have been accomplished. The significant contributions of the present research work include:

5.2.1 Journal papers:

1. Y.N. Zhang, D. Kevorkov, J. Li, E. Essadiqi, M. Medraj, Determination of the Solubility Range and Crystal Structure of the Mg-rich Ternary Compound in the Ca-Mg-Zn System, accepted by *Intermetallics*, Vol. 18, No. 12, 2010, pp. 2402-2411.
2. Y.N. Zhang, D. Kevorkov, F. Bridier, M. Medraj, Experimental investigation of the Ca-Mg-Zn system via diffusion couples and key experiments, submitted to *Intermetallics*, 2010.
3. Y.N. Zhang, D. Kevorkov, F. Bridier, X.D. Liu, M. Medraj, Solubility range and crystal structure determination of $Ca_2Mg_5Zn_{13}$ solid solution via SEM, EPMA, XRD, EBSD and TEM, will be submitted to *Scripta Materialia.*
4. Y.N. Zhang, D. Kevorkov, M. Medraj, New intermetallic compounds in Ca-Mg-Zn system, will be submitted to *Material Letters*.

5.2.2 Conference paper:

1. Y.N. Zhang, D. Kevorkov, J. Li, E. Essadiqi, M. Medraj, Experimental Determination of the Phase Equilibrium in the Ca-Mg-Zn system, submitted to *TOFA*, 2010.
2. Y.N. Zhang, D. Kevorkov, F. Bridier, M. Medraj, Morphological and Crystallographic Characterization of Ca-Mg-Zn Intermetallics in Ternary Diffusion Couples, submitted to *THERMEC*, 2011.

5.2.3 Oral presentation:

1. M. Medraj, D. Kevorkov, Y.N. Zhang, M.N. Khan, M. Aljarrah, Sk. Wasiur Rahman, Combinatorial Approach to the Development and Application of

Multicomponent Thermodynamic Database for the Mg Alloy Systems, *MS&T'10*, 2010 (invited).

2. Y.N. Zhang, D. Kevorkov, J. Li, E. Essadiqi, M. Medraj, Experimental Investigation of the Ca-Mg-Zn system via diffusion couples and key experiments, *CalphadXXXIX*, 2010, Jeju, Korea.
3. M. Medraj, Sk. Wasiur Rahman, D. Kevorkov, J. Li, E. Essadiqui, Y.N. Zhang, S. Konica and P. Chartrand, Thermodynamic Modeling and Experimental Investigations of the (Mg, Al)-Ca-Zn Systems, *CalphadXXXVIII*, 2009, Prague, Czech Republic.

5.3 Ongoing research and Future Work

The recommendations for further studies on the Mg-Ca-Zn system are summarized as follows:

1. The intrinsic diffusion coefficients and interdiffusion coefficients at the interfaces for this ternary system are still underway via diffusion couple technique at three different temperatures (300, 350, 400ºC) and different annealing times (3 days, 1 week, 2 weeks, 4 weeks).
2. Study the preferable crystal orientation of compounds formed by diffusion reaction and obtains the relations of crystal orientation and planes among equilibrium phases in the solid-state diffusion couples via EBSD.
3. The crystal structure determination of IM2 and IM4 ternary compounds is underway.
4. The Ca-Mg-Zn system should be re-optimized based on the current experimental results.

References

[1] X. F. Wan, Y. S. Sun, F Xue, J. Bai, W.J. Tao, Microstructure and mechanical properties of AZ62 based magnesium alloys with calcium addition, *Transactions of Nonferrous Metals Society of China*, Vol. 20, No. 5, 2010, pp. 757-762.

[2] M. Aljarrah, M. Medraj, X. Wang, E. Essadiqi, G. Dénès and A. Muntasar, Experimental Investigation of the Mg-Al-Ca System, *Journal of Alloys and Compounds*, Vol. 438, No. 1-2, 2007, pp. 131-141.

[3] O. Beffort, Ch. Hausmann, The Influence of Ca-additions on the Mechanical Properties of T300-C-Fibre/Mg (Al) Metal Matrix Composites, in: K.U. Kainer (Ed.), *Magnesium Alloys and their Applications*, 2000, pp. 215–220.

[4] A.A. Luo, Recent Magnesium Alloys Development for Elevated Temperature Application*, International Materials Review*, Vol.49, No.1, 2004, pp. 13-30.

[5] F. Nie and B.C. Muddle, Precipitation Hardening of Mg-Ca (-Zn) Alloys, *Scripta Materialia*, Vol.37, No.34, 1997, pp. 1475-1481.

[6] B. Zberg, P. J. Uggowitzer, and J. F. Löffler, MgZnCa Glasses Without Clinically Observable Hydrogen Evolution for Biodegradable Implants, *Nature Materials*, Published Online: 27th Sep. 2009.

[7] B. Zberg, E. R. Arataa, P. J. Uggowitzera, and J. F. Löffler, Tensile Properties of Glassy MgZnCa Wires and Reliability Analysis Using Weibull Statistics, *Acta Materialia*, Vol. 57, No. 11, 2009, pp. 3223-3231.

[8] U.R. Kattner, The Thermodynamic Modeling of Multicomponent Phase Equilibria, *Journal of Metals*, Vol. 49, No. 12, 1997, pp. 14-19.

[9] Y.A. Chang, S. Chen, F. Zhang, X. Yan, F. Xie, R. Schmid-Fetzer and W.A. Oates, Phase Diagram Calculation: Past, Present and Future, *Progress in Materials Science*, Vol.49, 2004, pp.313-345.

[10] L. Kaufman and H. Bernstein, "Computer calculation of phase diagrams with special reference to refractory metals", *Academic Press*, New York, 1970.

[11] K.C. Kumar, and P. Wollants, "Some guidelines for thermodynamic optimization of phase diagrams", *Journal of Alloys and Compounds*, vol. 320, 2001, pp. 189-198.

[12] S. Wasiur-Rahman and M. Medraj, Critical assessment and thermodynamic modeling of the binary Mg–Zn, Ca–Zn and ternary Mg–Ca–Zn systems, *Intermetallics*, Vol. 17, No. 10, 2009, pp. 847-864.

[13] “FactSage 6.0”, Thermfact (Centre for research in computational thermochemistry), Montreal, QC, Canada, 2010.

[14] R. Paris, Ternary Alloys, *Publications Scientifiques et Techniques du minist’ere de L’Air, Ministère de L’Air*, No.45, 1934, pp. 1-86.

[15] J.B. Clark, The Solid Constitution in the Mg-rich Region of the Mg-Ca-Zn Phase Diagram, *Trans. AIME*, Vol. 221,1961, pp. 644-645.

[16] J.B. Clark, *Joint Committee on Powder Diffraction Standards (JCPDS)* Card 12-0266, 1961.

[17] J.B. Clark, *Joint Committee on Powder Diffraction Standards (JCPDS)* Card 12-0569, 1961.

[18] T.V. Larinova, W.W. Park, and B.S. You, A Ternary Phase Observed in Rapid Solidified Mg-Ca-Zn alloys, *Scripta Materialia*, Vol. 45, 2001, pp. 7-12.

[19] P.M. Jardim, G. Solorzano, and J.B.V. Sande, Precipitate Crystal Structure Determination in Melt Spun Mg-1.5wt%Ca-6wt%Zn Alloy, *Mircoscopy and Microanaysis*, Vol. 8, 2002, pp. 487-496.

[20] P.M. Jardim, G. Solorzano, and J.B.V. Sande, Second Phase Formation in Melt-spun Mg-Ca-Zn Alloys, *Materials Science and Engineering A*, Vol. 381, No. 1-2, 2004, pp. 196-205.

[21] K. Oh-ishia, R. Watanabeb, C.L. Mendisa, and K. Hono, Age Hardening Response of Mg-0.3 at.% Ca alloys with different Zn contents, *Materials Science and Engineering: A*, Vol. 526, No. 1-2, 2009, pp. 177-184.

[22] C. O. Brubaker and Zi-Kui Liu, A computational thermodynamic model of the Ca–Mg–Zn system, *Journal of Alloys and Compounds*, Vol. 370, No. 1-2, 2004, pp. 114-122.

[23] J. S. Kirkaldy and L.C. Brown, Diffusion Behaviour in the Ternary, Multiphase Systems, *Canadian Metallurgical Quarterly*, Vol. 2, No. 1, 1963, pp. 90-115.

[24] J. B. Clark, Conventions for Plotting the Diffusion Paths in Multiphase Ternary Diffusion Couples on the Isothermal Section of a Ternary Phase Diagram, *Transactions of the Metallurgical Society of AIME*, Vol. 227, 1963, pp. 1250-1251.

[25] A.A. Kodentsov, G.F. Bastin, and F.J.J. van Loo, The Diffusion Couple Technique in Phase Diagram Determination, *Journal of Alloys and Compounds*, Vol. 320, No. 2, 2001, pp. 207-217.

[26] J.C. Zhao, A Combinatorial Approach for Structural Materials, *Advanced Engineering Materials*, Vol. 3, No. 3, 2001, pp. 143-147.

[27] J.C. Zhao, A Combinatorial Approach for Efficient Mapping of Phase Diagram and Properties, *Journal of Materials Research Society*, Vol. 16, No. 6, 2001, pp. 1565-1578.

[28] J.C. Zhao, M. R. Jackson, and L.A. Peluso, Determination of the Nb-Cr-Si Phase Diagram Using Diffusion Multiples, *Acta Materialia*, Vol. 51, No. 20, 2003, pp. 6395-6405.

[29] H.H. Xu, Y. Du, Y.C. Zhou, and Z.P. Jin, Determination of Phase Diagram Using the Diffusion Couple Technique, *Rare Metals*, Vol. 25, No. 5, 2006, pp.427-430.

[30] H. Putz, K. Brandenburg, Pearson's Crystal Data, Crystal Structure Database for Inorganic Compounds, CD-ROM software version 1.3.

[31] A.J. Schwartz, M. Kumar, B.L. Adams, Electron Backscatter Diffraction in Materials Science, Kluwer Academic/Plenum Publishers, Dordrecht/New York, 2000.

[32] J.J. Park and L.L.Wyman, Phase Relationships in Magnesium Alloys, *WADC Tech. Rept. 57-504*, Astia Document No. AD142110, 1957, pp. 1-27.

[33] F.J.J. van Loo and G.D. Rieck, Diffusion in the titanium-aluminium system—I. Interdiffusion between solid Al and Ti or Ti-Al alloys, *Acta Metallurgica*, Vol. 21, No. 1, 1973, pp. 61-71.

[34] F.J.J. van Loo and G.D. Rieck, Diffusion in the titanium-aluminium system—II. Interdiffusion in the composition range between 25 and 100 at.% Ti, *Acta Metallurgica*, Vol. 21, No. 1, 1973, pp. 73-84.

[35] B.Y. Kotur, M. Sikiritsa, O.I. Bodak, E.I. Gladyshevskii, Crystal structure of the compound $Sc_3Ni_{11}Si_4$, *Sov. Phys. Crystallogr*. Vol. 28, 1983, pp. 387-389.

[36] A.R. Denton and N.W. Ashcroft, Vegard's Law, *The American Physical Society*, Vol. 43, No. 6, 1991, pp. 3161-3164.

[37] D.W. Deng, K.H. Kuo, Z.P. Luo, D.J. Miller, M.J. Kramer and K.W. Dennis, Crystal structure of the hexagonal Zn_3MgY phase, *Journal of Alloys and Compounds*, Vol. 373, No, 1-2, 2004, pp. 156-160.

[38] W.D. Callister, Materials Science and Engineering: *An Introduction, John Wiley & Sons*, Inc, 2003.

[39] M. Latroche, P. Kalisvaart and P.H.L. Notten, Crystal structure of $Mg_{0.65}Sc_{0.35}Dx$ deuterides studied by X-ray and neutron powder diffraction, Journal of Solid State Chemistry, Vol. 179, No. 10, 2006, pp. 3024-3032.

[40] D. Kevorkov and M. Pekguleryuz, Experimental study of the Ce–Mg–Zn phase diagram at 350°C via diffusion couple technique, *Journal of Alloys and Compounds*, Vol. 478, No. 1-2, 2009, pp. 427-436.